infliximab-mediated action, we measured the concentration of soluble TNF. Only a small and similar amount of TNF was produced in WT mTNF, and S2A/S5A/S27A after 48 hours of incubation. Considering that infliximab is administered 1000 times more in molar ratio, it is concluded that soluble TNF does not interfere with the effect of infliximab by neutralization.

Our data clearly demonstrated that biologic effects—namely apoptosis, cell cycle arrest, and IL-10 production—are mediated by reverse signaling through mTNF only by infliximab, which might explain the difference in clinical effects between infliximab and etanercept in Crohn's disease. The expression of mTNF from the patients is substantially low compared with that of our transfectants. However, other transfectants expressing a less amount of mTNF were obtained during the process of clone selection. In even those transfectants, apoptosis was induced by infliximab but not by etanercept (data not shown). In addition, it is likely that activated primary T cells might be more susceptible to apoptosis or cell cycle arrest, compared with the T-cell line, Jurkat cells. Taken together, we suggest that reverse signals from mTNF might explain, at least in part, the cause of the differential clinical efficacy of infliximab vs. etanercept. The mechanism by which infliximab exerts a number of additional biologic effects through mTNF compared with etanercept is not clarified. However, considering that infliximab formed more stable complexes with mTNF on transfected cells with higher avidity than did etanercept,[37] infliximab might transmit stronger signals through mTNF into the cells expressing mTNF, thereby exerting a number of additional biologic effects compared with etanercept. In fact, cross-linking of etanercept bound to mTNF on Jurkat cells resulted in an increased apoptosis signal, although to a much lesser extent than with infliximab, as shown in Figure 5E.

IL-10 knockout mice develop bowel inflammation like Crohn's disease, and IL-10 is considered to be essential in regulating mucosal immunity.[38] Moreover, inflammatory bowel disease patients tend to have a low IL-10 producer genotype more often than normal controls,[39] and recombinant human IL-10 therapy showed clinical improvement.[40,41] Infliximab, not etanercept, induced IL-10 production from mTNF-expressing cells, attributing to control of the bowel immune system. This finding might be one of the mechanisms that explains the different clinical efficacy between these agents, in addition to induction of apoptosis and cell cycle arrest.

A functionally important intracellular motif of mTNF was assigned in this study. As shown in Figure 5C, S2A or S5A resulted in a pronounced decrease in the proportion of Annexin V-positive cells, whereas S27A alone did

not have any effect. Our observation that S2 and S5 are primarily important when assessed by apoptosis assay was supported by a previous report using a deletion mutant of mTNF.[15] The motif around S2 to S5 of mTNF (−SXXS−) has been shown to correspond to a target phosphorylation site of casein kinase I. The consensus sequence is conserved in several TNF ligand family proteins such as CD40L, CD30L, and FasL, which are reported to transduce "reverse signals," as in the case of mTNF.[42–44] Deletion of the N-terminal 13 aa residues including this casein kinase consensus motif resulted in the loss of intracellular calcium up-regulation elicited by mTNF stimulation.[15] In the current study, we identified for the first time the specific loci of mTNF critical for outside-to-inside signal transduction. Exploration of the similar functional significance of cytoplasmic Ser residues in the other TNF ligand family proteins would contribute to further investigation of the signal transduction mechanisms of "reverse signaling" in this cytokine family, which have not yet been clarified.

The dual role of mTNF for both cell cycle arrest and apoptosis is mediated by JNK activation, followed by activation of the cell cycle regulator p21$^{WAF1/CIP1}$ and the apoptosis-related proteins Bax and Bak and ROS. Considering that p21$^{WAF1/CIP1}$ and Bax are specific target proteins of p53[33,35] and ROS are shown to be the downstream mediator of p53-induced apoptosis,[45,46] it is likely that p53 is involved in the dual effect of infliximab. The time courses of JNK activation (Figure 9A), up-regulation of the p53-related molecules Bax and p21$^{WAF1/CIP1}$, and ROS activation (Figure 8B and 8C) suggest that p53 is downstream from JNK. The JNK pathway is activated by various extracellular stimuli, including stress and cytokines.[47] Activation of JNK leads to phosphorylation and the resultant activation of a number of transcription factors and molecules related to cell proliferation and apoptosis, including p53.[48] On the other hand, E-selectin expression, which was inducible by infliximab and etanercept, was independent of the JNK-p53 pathway because the JNK inhibitor SP600125 did not abolish E-selectin expression. Taken together with our previous report,[16] the molecular events essential for mTNF-mediated E-selectin expression remain to be clarified. It is of interest that p53 is associated with the cytoplasmic domain of CD40L and is involved in the clustering of CD40L,[49] one of the TNF ligand family proteins carrying the casein kinase I motif in its cytoplasmic domain, like mTNF.[15]

In conclusion, we demonstrated that outside-to-inside (reverse) signaling through mTNF was induced by infliximab, which resulted in the activation of JNK/p53 and the up-regulation of such molecules as Bax, Bak,

ROS, IL-10, and p21$^{\text{WAF1/CIP1}}$. Ser residues in the cytoplasmic domain of mTNF were essential for apoptosis and cell cycle arrest induced by the reverse signal. It has recently been reported that overexpression of p21$^{\text{WAF1/Cip1}}$ resulted in the down-regulation of a number of proinflammatory molecules in rheumatoid synovial fibroblasts.[50] It is thus suggested that the reverse signal through mTNF acts in concert to suppress mTNF-bearing cells through apoptosis, cell cycle arrest, and modulation of cytokine expression when strongly stimulated by such molecules as Ab (infliximab). Elucidation of the bipolar function of mTNF both as a ligand and a receptor will contribute to understanding the pathogenesis of local inflammation and the mechanisms of anti-TNF therapy as well as to identify a novel therapeutic target(s) in inflammation.

References

1. Black RA, Rauch CT, Kozlosky CJ, Peschon JJ, Slack JL, Wolfson MF, Castner BJ, Stocking KL, Reddy P, Srinivasan S, Nelson N, Boiani N, Schooley KA, Gerhart M, Davis R, Fitzner JN, Johnson RS, Paxton RJ, March CJ, Cerretti DP. A metalloproteinase disintegrin that releases tumour necrosis factor-α from cells. Nature 1997;385:729–733.
2. Moss ML, Jin SL, Milla ME, Bickett DM, Burkhart W, Carter HL, Chen WJ, Clay WC, Didsbury JR, Hassler D, Hoffman CR, Kost TA, Lambert MH, Leesnitzer MA, McCauley P, McGeehan G, Mitchell J, Moyer M, Pahel G, Rocque W, Overton LK, Schoenen F, Seaton T, Su JL, Becherer JD, et al. Cloning of a disintegrin metalloproteinase that processes precursor tumour-necrosis factor-alpha. Nature 1997; 385:733–736.
3. Old LJ. Tumor necrosis factor (TNF). Science 1985;230:630–632.
4. Vassalli P. The pathophysiology of tumor necrosis factors. Annu Rev Immunol 1992;10:411–452.
5. Vandenabeele P, Declercq W, Beyaert R, Fiers W. Two tumour necrosis factor receptors: structure and function. Trends Cell Biol 1995;5:392–399.
6. Caron G, Delneste Y, Aubry JP, Magistrelli G, Herbault N, Blaecke A, Meager A, Bonnefoy JY, Jeannin P. Human NK cells constitutively express membrane TNF-α (mTNF-α) and present mTNF-α-dependent cytotoxic activity. Eur J Immunol 1999;29:3588–3595.
7. Decker T, Lohmann-Matthes ML, Gifford GE. Cell-associated tumor necrosis factor (TNF) as a killing mechanism of activated cytotoxic macrophages. J Immunol 1987;138:957–962.
8. Parry SL, Sebbag M, Feldmann M, Brennan FM. Contact with T cells modulates monocyte IL-10 production: role of T cell membrane TNF-α. J Immunol 1997;158:3673–3681.
9. Kriegler M, Perez C, DeFay K, Albert I, Lu SD. A novel form of TNF/cachectin is a cell surface cytotoxic transmembrane protein: ramifications for the complex physiology of TNF. Cell 1988;53: 45–53.
10. Macchia D, Almerigogna F, Parronchi P, Ravina A, Maggi E, Romagnani S. Membrane tumour necrosis factor-α is involved in the polyclonal B-cell activation induced by HIV-infected human T cells. Nature 1993;363:464–466.
11. Higuchi M, Nagasawa K, Horiuchi T, Oike M, Ito Y, Yasukawa M, Niho Y. Membrane tumor necrosis factor-α (TNF-α) expressed on HTLV-I-infected T cells mediates a costimulatory signal for B cell activation—characterization of membrane TNF-α. Clin Immunol Immunopathol 1997;82:133–140.
12. Grell M, Douni E, Wajant H, Lohden M, Clauss M, Maxeiner B, Georgopoulos S, Lesslauer W, Kollias G, Pfizenmaier K, et al. The transmembrane form of tumor necrosis factor is the prime acti-

vating ligand of the 80 kDa tumor necrosis factor receptor. Cell 1995;83:793–802.
13. Lou J, Dayer JM, Grau GE, Burger D. Direct cell/cell contact with stimulated T lymphocytes induces the expression of cell adhesion molecules and cytokines by human brain microvascular endothelial cells. Eur J Immunol 1996;26:3107–3113.
14. Aversa G, Punnonen J, de Vries JE. The 26-kD transmembrane form of tumor necrosis factor α on activated CD4+ T cell clones provides a costimulatory signal for human B cell activation. J Exp Med 1993;177:1575–1585.
15. Watts AD, Hunt NH, Wanigasekara Y, Bloomfield G, Wallach D, Roufogalis BD, Chaudhri G. A casein kinase I motif present in the cytoplasmic domain of members of the tumour necrosis factor ligand family is implicated in "reverse signalling." EMBO J 1999; 18:2119–2126.
16. Harashima S, Horiuchi T, Hatta N, Morita C, Higuchi M, Sawabe T, Tsukamoto H, Tahira T, Hayashi K, Fujita S, Niho Y. Outside-to-inside signal through the membrane TNF-α induces E-selectin (CD62E) expression on activated human CD4+ T cells. J Immunol 2001; 166:130–136.
17. Lohrengel B, Lu M, Roggendorf M. Molecular cloning of the woodchuck cytokines: TNF-α, IFN-γ, and IL-6. Immunogenetics 1998;47:332–335.
18. Pocsik E, Duda E, Wallach D. Phosphorylation of the 26 kDa TNF precursor in monocytic cells and in transfected HeLa cells. J Inflamm 1995;45:152–160.
19. Bathon JM, Martin RW, Fleischmann RM, Tesser JR, Schiff MH, Keystone EC, Genovese MC, Wasko MC, Moreland LW, Weaver AL, Markenson J, Finck BK. A comparison of etanercept and methotrexate in patients with early rheumatoid arthritis. N Engl J Med 2000; 343:1586–1593.
20. Lipsky PE, van der Heijde DM, St. Clair EW, Furst DE, Breedveld FC, Kalden JR, Smolen JS, Weisman M, Emery P, Feldmann M, Harriman GR, Maini RN. Infliximab and methotrexate in the treatment of rheumatoid arthritis. Anti-Tumor Necrosis Factor Trial in Rheumatoid Arthritis with Concomitant Therapy Study Group. N Engl J Med 2000; 343:1594–1602.
21. Targan SR, Hanauer SB, van Deventer SJ, Mayer L, Present DH, Braakman T, DeWoody KL, Schaible TF, Rutgeerts PJ. A short-term study of chimeric monoclonal antibody cA2 to tumor necrosis factor α for Crohn's disease. Crohn's Disease cA2 Study Group. N Engl J Med 1997;337:1029–1035.
22. Mease PJ, Goffe BS, Metz J, VanderStoep A, Finck B, Burge DJ. Etanercept in the treatment of psoriatic arthritis and psoriasis: a randomised trial. Lancet 2000;356:385–390.
23. Gorman JD, Sack KE, Davis JC Jr. Treatment of ankylosing spondylitis by inhibition of tumor necrosis factor α. N Engl J Med 2002;346:1349–1356.
24. Braun J, Brandt J, Listing J, Zink A, Alten R, Golder W, Gromnica-Ihle E, Kellner H, Krause A, Schneider M, Sorensen H, Zeidler H, Thriene W, Sieper J. Treatment of active ankylosing spondylitis with infliximab: a randomised controlled multicentre trial. Lancet 2002;359: 1187–1193.
25. Munoz-Fernandez S, Hidalgo V, Fernandez-Melon J, Schlincker A, Martin-Mola E. Effect of infliximab on threatening panuveitis in Behçet's disease. Lancet 2001;358:1644.
26. Knight DM, Trinh H, Le J, Siegel S, Shealy D, McDonough M, Scallon B, Moore MA, Vilcek J, Daddona P, et al. Construction and initial characterization of a mouse-human chimeric anti-TNF antibody. Mol Immunol 1993;30:1443–1453.
27. Mohler KM, Torrance DS, Smith CA, Goodwin RG, Stremler KE, Fung VP, Madani H, Widmer MB. Soluble tumor necrosis factor (TNF) receptors are effective therapeutic agents in lethal endotoxemia and function simultaneously as both TNF carriers and TNF antagonists. J Immunol 1993;151:1548–1561.

28. Mitoma H, Horiuchi T, Tsukamoto H. Binding activities of inflix-imab and etanercept to transmembrane tumor necrosis factor-α. Gastroenterology 2004;126:934–935.

29. Sandborn WJ, Hanauer SB, Katz S, Safdi M, Wolf DG, Baerg RD, Tremaine WJ, Johnson T, Diehl NN, Zinsmeister AR. Etanercept for active Crohn's disease: a randomized, double-blind, placebo-controlled trial. Gastroenterology 2001;121:1088–1094.

30. Himeji D, Horiuchi T, Tsukamoto H, Hayashi K, Watanabe T, Harada M. Characterization of caspase-8L: a novel isoform of caspase-8 that behaves as an inhibitor of the caspase cascade. Blood 2002;99:4070–4078.

31. Van den Brande JM, Braat H, van den Brink GR, Versteeg HH, Bauer CA, Hoedemaeker I, van Montfrans C, Hommes DW, Pep-pelenbosch MP, van Deventer SJ. Infliximab but not etanercept induces apoptosis in lamina propria T-lymphocytes from patients with Crohn's disease. Gastroenterology 2003;124:1774–1785.

32. Lugering A, Schmidt M, Lugering N, Pauels HG, Domschke W, Kucharzik T. Infliximab induces apoptosis in monocytes from patients with chronic active Crohn's disease by using a caspase-dependent pathway. Gastroenterology 2001;121:1145–1157.

33. Miyashita T, Reed JC. Tumor suppressor p53 is a direct transcrip-tional activator of the human bax gene. Cell 1995;80:293–299.

34. Kannan K, Amariglio N, Rechavi G, Jakob-Hirsch J, Kela I, Kaminski N, Getz G, Domany E, Givol D. DNA microarrays identification of primary and secondary target genes regulated by p53. Oncogene 2001;20:2225–2234.

35. el-Deiry WS, Tokino T, Velculescu VE, Levy DB, Parsons R, Trent JM, Lin D, Mercer WE, Kinzler KW, Vogelstein B. WAF1, a potential mediator of p53 tumor suppression. Cell 1993;75:817–825.

36. Cornillie F, Shealy D, D'Haens G, Geboes K, Van Assche G, Ceuppens J, Wagner C, Schaible T, Plevy SE, Targan SR, Rut-geerts P. Infliximab induces potent anti-inflammatory and local immunomodulatory activity but no systemic immune suppression in patients with Crohn's disease. Aliment Pharmacol Ther 2001; 15:463–473.

37. Scallon B, Cai A, Solowski N, Rosenberg A, Song XY, Shealy D, Wagner C. Binding and functional comparisons of two types of tumor necrosis factor antagonists. J Pharmacol Exp Ther 2002; 301:418–426.

38. Kuhn R, Lohler J, Rennick D, Rajewsky K, Muller W. Interleukin-10-deficient mice develop chronic enterocolitis. Cell 1993;75: 263–274.

39. Tagore A, Gonsalkorale WM, Pravica V, Hajeer AH, McMahon R, Whorwell PJ, Sinnott PJ, Hutchinson IV. Interleukin-10 (IL-10) genotypes in inflammatory bowel disease. Tissue Antigens 1999; 54:386–390.

40. Fedorak RN, Gangl A, Elson CO, Rutgeerts P, Schreiber S, Wild G, Hanauer SB, Kilian A, Cohard M, LeBeaut A, Feagan B. Recom-binant human interleukin 10 in the treatment of patients with mild to moderately active Crohn's disease. The Interleukin 10 Inflammatory Bowel Disease Cooperative Study Group. Gastroen-terology 2000;119:1473–1482.

41. Schreiber S, Fedorak RN, Nielsen OH, Wild G, Williams CN, Nikolaus S, Jacyna M, Lashner BA, Gangl A, Rutgeerts P, Isaacs K, van Deventer SJ, Koningsberger JC, Cohard M, LeBeaut A, Hanauer SB. Safety and efficacy of recombinant human interleu-kin 10 in chronic active Crohn's disease. Crohn's Disease IL-10 Cooperative Study Group. Gastroenterology 2000;119: 1461–1472.

42. van Essen D, Kikutani H, Gray D. CD40 ligand-transduced co-stimulation of T cells in the development of helper function. Nature 1995;378:620–623.

43. Wiley SR, Goodwin RG, Smith CA. Reverse signaling via CD30 ligand. J Immunol 1996;157:3635–3639.

44. Suzuki I, Fink PJ. The dual functions of fas ligand in the regulation of peripheral CD8+ and CD4+ T cells. Proc Natl Acad Sci U S A 2000;97:1707–1712.

45. Lotem J, Peled-Kamar M, Groner Y, Sachs L. Cellular oxidative stress and the control of apoptosis by wild-type p53, cytotoxic compounds, and cytokines. Proc Natl Acad Sci U S A 1996;93: 9166–9171.

46. Johnson TM, Yu ZX, Ferrans VJ, Lowenstein RA, Finkel T. Reactive oxygen species are downstream mediators of p53-dependent apoptosis. Proc Natl Acad Sci U S A 1996;93:11848–11852.

47. Ip YT, Davis RJ. Signal transduction by the c-Jun N-terminal kinase (JNK)—from inflammation to development. Curr Opin Cell Biol 1998;10:205–219.

48. Buschmann T, Potapova O, Bar-Shira A, Ivanov VN, Fuchs SY, Hen-derson S, Fried VA, Minamoto T, Alarcon-Vargas D, Pincus MR, Gaarde WA, Holbrook NJ, Shiloh Y, Ronai Z. Jun NH2-terminal ki-nase phosphorylation of p53 on Thr-81 is important for p53 stabi-lization and transcriptional activities in response to stress. Mol Cell Biol 2001;21:2743–2754.

49. Grassme H, Bock J, Kun J, Gulbins E. Clustering of CD40 ligand is required to form a functional contact with CD40. J Biol Chem 2002;277:30289–30299.

50. Nonomura Y, Kohsaka H, Nagasaka K, Miyasaka N. Gene trans-fer of a cell cycle modulator exerts anti-inflammatory effects in the treatment of arthritis. J Immunol 2003;171:4913–4919.

Brief report

Allogeneic stem-cell transplantation with reduced conditioning intensity as a novel immunotherapy and antiviral therapy for adult T-cell leukemia/lymphoma

Jun Okamura, Atae Utsunomiya, Ryuji Tanosaki, Naokuni Uike, Shunro Sonoda, Mari Kannagi, Masao Tomonaga, Mine Harada, Nobuhiro Kimura, Masato Masuda, Fumio Kawano, Yuji Yufu, Hiroyoshi Hattori, Hiroshi Kikuchi, and Yoshio Saburi

Sixteen patients with adult T-cell leukemia/lymphoma (ATL) who were all over 50 years of age underwent allogeneic stem cell transplantation with reduced-conditioning intensity (RIST) from HLA-matched sibling donors after a conditioning regimen consisting of fludarabine (180 mg/m²), busulfan (8 mg/kg), and rabbit antithymocyte globulin (5 mg/kg). The observed regimen-related toxicities and nonhematologic toxicities were all found to be acceptable. Disease relapse was the main cause of treatment failure. Three patients who had a relapse subsequently responded to a rapid discontinuation of the immunosuppressive agent and thereafter achieved another remission. After RIST, the human T-cell leukemia virus type 1 (HTLV-1) proviral load became undetectable in 8 patients. RIST is thus considered to be a feasible treatment for ATL. Our data also suggest the presence of a possible graft-versus-ATL effect; an anti-HTLV-1 activity was also found to be associated with this procedure. (Blood. 2005;105:4143-4145)

© 2005 by The American Society of Hematology

Introduction

Therapeutic trials to improve the dismal prognosis of adult T-cell leukemia/lymphoma (ATL) among elderly persons who are infected with human T-lymphotropic virus type 1 (HTLV-1) have so far been unsuccessful.[1-5] However, there have been a few encouraging reports on allogeneic stem cell transplantation (alloSCT) for selected populations of patients with ATL.[6-9] Although most of the patients who were treated successfully in these studies received grafts from HLA-identical siblings and the patients were younger than the average age for patients with ATL, the main cause of treatment failure after alloSCT remains transplant-related complications such as acute graft-versus-host disease (aGVHD). Recent advances have now allowed alloSCT to be extended to older patients through the use of reduced-intensity conditioning regimens.[10-12] We therefore conducted a phase 1 clinical trial of alloSCT with reduced-conditioning intensity (RIST) to clarify whether this newly developed procedure is feasible for ATL patients over 50 years of age.

Study design

The eligible patients ranged from 50 to 70 years of age and met the diagnostic criteria for ATL.[13] The patients were required to be in either complete remission (CR) or partial remission (PR) at the time of registration[5] and to have an HLA-identical sibling donor. All patients and donors gave their written informed consent to participate in this study, which was approved by the institutional review board of each participating institution.

The conditioning regimen consisted of fludarabine (180 mg/m²), busulfan (8 mg/kg), and rabbit antithymocyte globulin (ATG; 5 mg/kg) as reported.[10] Granulocyte colony-stimulating factor-mobilized peripheral blood (PB) grafts from the donors were transplanted. To prevent GVHD, cyclosporine (CsA) was administered intravenously (3 mg/kg/d). The severity of GVHD was graded according to the consensus criteria.[14] The degrees of donor-recipient chimerism and HTLV-1 proviral DNA in PB mononuclear cells (MNCs) were quantified according to published methods.[15,16] The primary end points of this study were either engraftment, as judged by the achievement of complete donor chimerism before day 90, or the occurrence of early transplant-related mortality (TRM) before day 100 after RIST. We therefore registered 16 patients according to the Simon 2-step design.[17] The overall survival (OS) and event-free survival (EFS) were estimated by the Kaplan-Meier method. The log-rank test was used to compare the OS and EFS between the subgroups.

Results and discussion

Clinical results

The median ages of the patients and donors were 57 and 54 years, respectively. Because one patient (UPN11) received extra medication during the conditioning phase due to rapid disease progression, the patient was considered as evaluable only for engraftment. One

Table 1. Patient characteristics and outcomes

| UPN | Age, y/sex | ATL subtype | Donor HTLV-1 antibody | Complete chimerism, PB MNCs, > 90% of donor cells, d | GVHD | | HTLV-1 proviral load | | Outcome | Survival, d |
					Acute	Chronic	Before RIST	After RIST, lowest level		
1	67/F	Acute	+	No	0	NE	292	68	LN relapse, d 47, DOD	135
2	61/F	Acute	−	14	IV	No	> 1000	2	LN relapse, d 47, CR after d/c CsA, died of aGVHD	173
3	62/F	Lymphoma	+	28	0	NE	30	43	LN relapse, d 14, DOD	43
4	62/M	Acute	+	14	1	Yes	> 1000	< 0.5	LN and skin relapse, d 28 and CR after d/c CsA	> 1214
5	51/M	Acute	−	42	0	No	709	223	LN and skin relapse, d 21, PR after d/c CsA, DOD	173
6	66/F	Acute	+	14	II	Yes	798	7	CR	> 1177
7	51/M	Acute	−	14	II	Yes	27	< 0.5	CR	> 1162
8	55/F	Lymphoma	+	20	0	No	331	67	LN relapse, d 74, DOD	201
9	53/M	Lymphoma	−	17	II	Yes	236	< 0.5	CR	> 1017
10	54/M	Lymphoma	−	17	II	Yes	440	< 0.5	LN relapse, d 171, CR after chemoradiotherapy	> 910
11	55/M	Acute	+	21	NE	NE	214	NE	NE	NE
12	66/F	Acute	−	14	0	Yes	> 1000	< 0.5	Died of cGVHD and infection	285
13	57/M	Acute	+	15	III	No	> 1000	2	LN and lung relapse, d 182, DOD	266
14	67/F	Lymphoma	−	15	III	No	582	< 0.5	LN relapse, d 62, DOD	219
15	54/M	Acute	+	28	III	NE	> 1000	< 0.5	Died of aGVHD and sepsis	71
16	56/M	Acute	−	14	IV	No	> 1000	< 0.5	Died of aGVHD	126

patient (UPN1) who developed an early relapse failed to achieve complete donor chimerism before day 90 (Table 1). Therefore, 15 of 16 patients were considered to demonstrate successful results for engraftment. Another patient (UPN15) developed early TRM on day 71 after RIST. As previously reported for this regimen, the regimen-related toxicities and hematologic toxicity were all acceptable. No grade 4 nonhematologic toxicity was observed.[10,18,19] Two patients developed fatal grade IV aGVHD while they were not receiving CsA because of an absence of aGVHD and an early disease relapse. Regarding major infectious complications, sepsis in 2 patients, a reactivation of cytomegalovirus in 13, and an Epstein-Barr virus-associated lymphoproliferative disorder in 2 were observed. Of the 12 patients who could be evaluated regarding the response to RIST, 9 exhibited CR at 30 days after RIST. Although the underlying mechanisms are unclear, the CR was considered most likely to be due to the chemotherapeutic effect, the graft-versus-ATL effect, or a combination of both. Disease relapse occurred in 9 patients. Interestingly, 3 patients who had a relapse subsequently achieved a second CR or PR after the rapid discontinuation of CsA. As of December 31, 2004, 5 patients are alive, and 10 had died of either ATL (6) or TRM (4). In all cases, TRM was considered to be related to GVHD (Table 1). The EFS and OS for the 15 patients at 2 years are 20.0% ± 10.3% and 33.3 ± 12.2%, respectively. The OS for patients who did and did not develop aGVHD was 50.0% ± 15.8% and 0%, respectively (P = .06).

Kinetics of the HTLV-1 proviral load after RIST

The HTLV-1 proviral load decreased to an undetectable level (< 0.5 copies) within 3 months after RIST in 8 patients, specifically, 6 of 8 patients who received grafts from HTLV-1 antibody-

negative donors and 2 of 7 patients whose donors were virus carriers (Figure 1). Four of the 5 patients who survived more than 18 months presently continue to demonstrate an undetectable HTLV-1 proviral load. The other long-term survivor whose donor was a carrier (UPN6) showed a high HTLV-1 proviral load without any disease relapse beyond 18 months.

In this first prospective study of RIST for ATL, we clearly demonstrated that RIST from HLA-matched sibling donors is a feasible therapeutic procedure for patients over 50 years of age, as has been reported for other lymphoid malignancies.[20-22] However, the TRM of 27% was not negligible. Notably, 2 of 4 TRMs were related to grade IV aGVHD, and they were induced by a
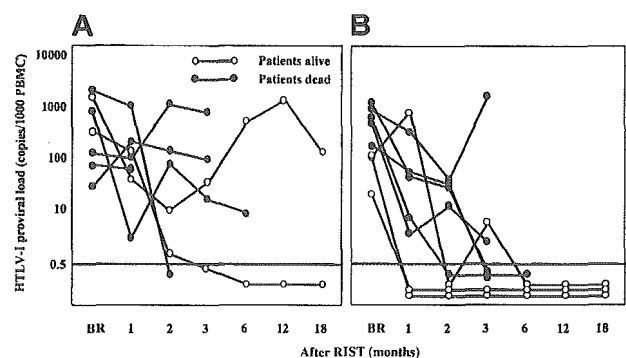

Figure 1. The kinetics of the HTLV-1 proviral load after RIST by different types of donors. Panel B indicates transplants from HTLV-1⁻ donors; panel A shows results from HTLV-1⁺ carrier donors. The HTLV-1 proviral load was expressed as copies per 1000 MNCs. A load of less than 0.5 copies/1000 MNCs was considered to be undetectable. ○ indicates patients still alive at end of study; ●, patients that died during study. BR indicates before RIST. The horizontal line at 0.5 indicates detection limit. PBMNC indicates peripheral blood mononuclear cell.

discontinuation of CsA, which indicated the difficulty in the tapering or discontinuation of CsA in RIST. Interestingly, 3 patients who had a relapse responded to a rapid discontinuation of the immunosuppressive agent CsA. Although the difference was not statistically significant, the patients who developed aGVHD tended to show a better OS than those who did not ($P = .06$). These observations thus suggest the presence of a graft-versus-ATL effect in RIST. The dramatic decrease in the HTLV-1 proviral load to an undetectable level after RIST in more than half the patients was unexpected. Similar results, which demonstrated an antiviral effect by SCT for ATL, have been previously described in case reports.[23,24] Two patients who received grafts from HTLV-1^{+} donors also became negative for viral load after RIST. The uninfected normal donor T cells present in the graft might have overwhelmed the HTLV-1–infected T cells in the unique environment after transplantation. In one patient (UPN6) who received a graft from an HTLV-1^{+} carrier donor, an increase in the HTLV-1 proviral load without disease relapse was observed beyond 1 year after RIST. The proviral load gradually returned to the donor level after the second year. A temporary proliferation of HTLV-I–infected (nonclonal) donor cells might have occurred due to some unknown etiology.

We have herein shown that RIST is a feasible treatment procedure for ATL patients over 50 years of age. The possible presence of a graft-versus-ATL effect as well as anti–HTLV-1 activity for RIST were also observed. Ganciclovir and prophylactic oral acyclovir were the antiviral agents used in the study. They are effective only for herpes virus and not for retrovirus, and therefore, they possess a negligible anti–HTLV-1 activity. In a separate analysis in this study, Harashima et al found the presence of an HLA class I restricted proliferation of CD8^{+} cytotoxic T lymphocytes (CTLs), which exhibited a specific reactivity to a certain epitope of the HTLV-1 regulatory protein Tax.[25] These Tax-specific CTLs might therefore play a critical role in eradicating ATL cells in vivo. These results indicate that RIST may be applicable as a new modality for the future treatment for other virus-induced diseases that have a poor prognosis.

References

1. Uchiyama T, Yodoi J, Sagawa K, et al. Adult T-cell leukemia: clinical and hematological features of 16 cases. Blood. 1977;50:481-492.

2. Shimoyama M, Ota K, Kikuchi M, et al. Major prognostic factors of adult patients with advanced T-cell lymphoma/leukemia. J Clin Oncol. 1988;6:1088-1097.

3. Uozumi K, Hanada S, Ohno N, et al. Combination chemotherapy (RCM protocol: response-oriented cyclic multidrug protocol) for the acute or lymphoma type adult T-cell leukemia. Leuk Lymphoma. 1995;18:317-323.

4. Gill PS, Harrington WJ, Kaplan MH, et al. Treatment of adult T-cell leukemia-lymphoma with a combination of interferon alfa and zidovudine. N Engl J Med. 1995;332:1744-1748.

5. Yamada Y, Tomonaga M, Fukuda H, et al. A new G-CSF-supported combination chemotherapy, LSG15, for adult T-cell leukaemia-lymphoma: Japan Clinical Oncology Group Study 9303. Br J Haematol. 2001;113:375-382.

6. Sobue R, Yamauchi T, Miyamura K, et al. Treatment of adult T cell leukemia with mega-dose cyclophosphamide and total body irradiation followed by allogeneic bone marrow transplantation. Bone Marrow Transplant. 1987;2:441-444.

7. Borg A, Liu Yin JA, Johnson PRE, et al. Successful treatment of HTLV-I-associated adult T-cell leukaemia lymphoma by allogeneic bone marrow transplantation. Br J Haematol. 1996;94:713-715.

8. Utsunomiya A, Miyazaki Y, Takatsuka Y, et al. Improved outcome of adult T cell leukemia/lymphoma with allogeneic hematopoietic stem cell transplantation. Bone Marrow Transplant. 2001;27:15-20.

9. Kami M, Hamaki T, Miyakoshi S, et al. Allogeneic haematopoietic stem cell transplantation for the treatment of adult T-cell leukaemia/lymphoma. Br J Haematol. 2003;120:304-309.

10. Slavin S, Nagler A, Naparstek E, et al. Nonmyeloablative stem cell transplantation and cell therapy as an alternative to conventional bone marrow transplantation with lethal cytoreduction for the treatment of malignant and nonmalignant hematologic diseases. Blood. 1998;91:756-763.

11. Khouri IF, Keating M, Korbling M, et al. Transplant-lite: induction of graft-versus-malignancy using fludarabine-based nonablative chemotherapy and allogeneic blood progenitor-cell transplantation as treatment for lymphoid malignancies. J Clin Oncol. 1998;16:2817-2824.

12. Childs R, Chernoff A, Contentin N, et al. Regression of metastatic renal-cell carcinoma after nonmyeloablative allogeneic peripheral-blood stem-cell transplantation. N Engl J Med. 2000;343:750-758.

13. Shimoyama, M. The Lymphoma Study Group: diagnostic criteria and classification of clinical subtypes of adult T-cell leukemia-lymphoma. Br J Haematol. 1991;79:428-437.

14. Przepiorka D, Weisdorf D, Martin P, et al. Report of the 1994 consensus conference on acute GVHD grading. Bone Marrow Transplant. 1995;15:825-828.

15. Thiede C, Florek M, Bornhauser M, et al. Rapid quantification of mixed chimerism using multiplex amplification of short tandem repeat markers and fluorescence detection. Bone Marrow Transplant. 1999;23:1055-1060.

16. Sonoda J, Koriyama C, Yamamoto S, et al. HTLV-1 provirus load in peripheral blood lymphocytes of HTLV-1 carriers is diminished by green tea drinking. Cancer Sci. 2004;95:596-601.

17. Simon R, Wittes RE. Methodologic guidelines for reports of clinical trials. Cancer Treat Rep. 1985;69:1-3.

18. Massenkeil G, Nagy M, Lawang M, et al. Reduced intensity conditioning and prophylactic DLI can cure patients with high-risk leukemias if complete donor chimerism can be achieved. Bone Marrow Transplant. 2003;31:339-345.

19. Schetelig J, Bornhauser M, Kiehl M, et al. Reduced-intensity conditioning with busulfan and fludarabine with or without antithymocyte globulin in HLA-identical sibling transplantation—a retrospective analysis. Bone Marrow Transplant. 2004;33:483-490.

20. Kogel KE, McSweeney PA. Reduced-intensity allogeneic transplantation for lymphoma. Curr Opin Oncol. 2002;14:475-483.

21. Khouri IF, Lee MS, Saliba RM, et al. Nonablative allogeneic stem-cell transplantation for advanced/recurrent mantle-cell lymphoma. J Clin Oncol. 2003;21:4407-4412.

22. Niederwieser D, Maris M, Shizuru JA, et al. Low-dose total body irradiation (TBI) and fludarabine followed by hematopoietic cell transplantation (HCT) from HLA-matched or mismatched unrelated donors and postgrafting immunosuppression with cyclosporine and mycophenolate mofetil (MMF) can induce durable complete chimerism and sustained remissions in patients with hematological diseases. Blood. 2003;101:1620-1629.

23. Abe Y, Yashiki S, Choi I, et al. Eradication of virus-infected T-cells in a case of adult T-cell leukemia/lymphoma by nonmyeloablative peripheral blood stem cell transplantation with conditioning consisting of low-dose total body irradiation and pentostatin. Int J Hematol. 2002;76:91-93.

24. Ogata M, Ogata Y, Imamura T, et al. Successful bone marrow transplantation from an unrelated donor in a patient with adult T cell leukemia. Bone Marrow Transplant. 2002;30:699-701.

25. Harashima N, Kurihara K, Utsunomiya A, et al. Graft-versus-human Tax response in adult T cell leukemia patients after hematopoietic stem cell transplantation. Cancer Res. 2004;64:391-399.

Development of functional human blood and immune systems in NOD/SCID/IL2 receptor γ chain^null mice

Fumihiko Ishikawa, Masaki Yasukawa, Bonnie Lyons, Shuro Yoshida, Toshihiro Miyamoto, Goichi Yoshimoto, Takeshi Watanabe, Koichi Akashi, Leonard D. Shultz, and Mine Harada

Here we report that a new nonobese diabetic/severe combined immunodeficient (NOD/SCID) mouse line harboring a complete null mutation of the common cytokine receptor γ chain (NOD/SCID/interleukin 2 receptor [IL2r] γ^null) efficiently supports development of functional human hemato-lymphopoiesis. Purified human (h) CD34+ or hCD34+hCD38− cord blood (CB) cells were transplanted into NOD/SCID/IL2rγ^null newborns via a facial vein. In all recipients injected with 10^5 hCD34+ or 2×10^4 hCD34+hCD38− CB cells, human hematopoietic cells were reconstituted at approximately 70% of chimerisms. A high percentage of the human hematopoietic cell chimerism persisted for more than 24 weeks after transplantation, and hCD34+ bone marrow grafts of primary recipients could reconstitute hematopoiesis in secondary NOD/SCID/IL2rγ^null recipients, suggesting that this system can support self-renewal of human hematopoietic stem cells. hCD34+hCD38− CB cells differentiated into mature blood cells, including myelomonocytes, dendritic cells, erythrocytes, platelets, and lymphocytes. Differentiation into each lineage occurred via developmental intermediates such as common lymphoid progenitors and common myeloid progenitors, recapitulating the steady-state human hematopoiesis. B cells underwent normal class switching, and produced antigen-specific immunoglobulins (Igs). T cells displayed the human leukocyte antigen (HLA)–dependent cytotoxic function. Furthermore, human IgA-secreting B cells were found in the intestinal mucosa, suggesting reconstitution of human mucosal immunity. Thus, the NOD/SCID/IL2rγ^null newborn system might be an important experimental model to study the human hemato-lymphoid system. (Blood. 2005;106:1565-1573)

© 2005 by The American Society of Hematology

Introduction

To analyze human immune and hematopoietic development and function in vivo, a number of studies have been tried to reproduce human hematopoiesis in small animal xenotransplantation models.[1] Successful transplantation of human hematopoietic tissues in immune-compromised mice was first reported in late 1980s by using homozygous severe combined immunodeficient (C.B.17-SCID) mice. In the first model of a humanized lymphoid system in a SCID mouse (SCID-hu model), McCune et al simultaneously transplanted human fetal tissues, including fetal liver hematopoietic cells, thymus, and lymph nodes, into SCID mice and induced mature human T- and B-cell development.[2] Mosier et al successfully reconstituted human T and B cells by transferring human blood mononuclear cells into SCID mice.[3] These initial studies suggested the usefulness of immunodeficient mice for reconstitution of the human lymphoid system from human bone marrow hematopoietic stem cells (HSCs).

After these initial reports, a number of modified SCID models have been proposed to try to reconstitute human immunity.[4] In addition, recombination activating gene (RAG)–deficient strains have been used as recipients in xenotransplantation: T- and B-cell–deficient $Prkdc^{scid}$, $Rag1^{-/-}$, or $Rag2^{-/-}$ mutant mice[5-7] were capable of supporting engraftment of human cells. The engraftment levels in these models, however, were still low, presumably due to the remaining innate immunity of host animals.[1] Nonobese diabetic/severe combined immunodeficient (NOD/SCID) mice have been shown to support higher levels of human progenitor cell engraftment than BALB/c/SCID or C.B.17/SCID mice.[8] Levels of human cell engraftment were further improved by treating NOD/SCID mice with anti-asialo GM1 (gangliosidemonosialic acid) antibodies[9] that can abrogate natural killer (NK) cell activity. Recently, NOD/SCID mice harboring either a null allele at the β_2-microglobulin gene (NOD/SCID/$\beta 2m^{-/-}$)[10] or a truncated common cytokine receptor γ chain (γc) mutant lacking its cytoplasmic region (NOD/SCID/$\gamma_c^{-/-}$)[11,12] were developed. In these mice, NK- as well as T- and B-cell development and functions are disrupted, because $\beta 2m$ is necessary for major histocompatibility complex (MHC) class I–mediated innate immunity, and because γc (originally called IL-2Rγ chain) is an indispensable component

of receptor heterodimers for many lymphoid-related cytokines (ie, IL-2, IL-7, IL-9, IL-12, IL-15, and IL-21).[13] Injection of human bone marrow or cord blood (CB) cells into these mice resulted in successful generation of human T and B cells. In our hands, efficiencies of CB cell engraftment represented by percentages of circulating human (h) CD45$^+$ cells were significantly (2- to 5-fold) higher in NOD/SCID/β2m$^{-/-}$ newborns than those in adults (F.I., M.H., and L.D.S., unpublished data, April 2003). More recently, transplantation of hCD34$^+$ CB cells into Rag2$^{-/-}$ γc$^{-/-}$ newborns regenerated adaptive immunity mediated by functional T and B cells,[14] suggesting heightened support for xenogeneic transplants especially in the neonatal period. Efficiency of reconstitution of human hematopoiesis may be, however, still suboptimal in these models because chimerisms of human cells are not stable in each experiment.[11,12,14] Furthermore, there is little information regarding reconstitution of human myeloerythroid components in these xenogeneic models.

Two types of mouse lines with truncated or complete null γc mutant[15-17] have been reported. NOD/SCID/$\gamma_c$$^{-/-}$ and Rag2$^{-/-}$ γc$^{-/-}$ mouse strains harbor a truncated γc mutant lacking the intracellular domain,[15] and therefore, binding of γc-related cytokines to each receptor should normally occur in these models.[18] For example, IL-2R with the null γc mutations would be an $\alpha\beta$ heterodimer complex with an affinity approximately 10 times lower than that of the high affinity $\alpha\beta\gamma$ heterotrimer complex in mice with the truncated γc mutant.[19] γc has also been shown to dramatically increase the affinity to its ligands through the receptors for IL-4, IL-7, and IL-15.[20-23] Previous studies suggested that γc-related receptors including IL-2Rβ chain and IL-4Rα chain could activate janus-activated kinases (JAKs) to some extent in the presence of the extracellular domain of γc, independent of the cytoplasmic domain of γc.[24,25] Thus, in order to block the signaling through γc-related cytokine receptors more completely, we made NOD/SCID mice harboring complete null mutation of γc[16] (the NOD/SCID/IL2rγ^{null} strain). By using NOD/SCID/IL2rγ^{null} newborns, we successfully reconstituted myeloerythroid as well as lymphoid maturation by injecting human CB or highly-enriched CB HSCs at a high efficiency. Reconstitution of human hematopoiesis persisted for a long term. The developing lymphoid cells were functional for immunoglobulin (Ig) production and human leukocyte antigen (HLA)–dependent cytotoxic activity. Our data show that the NOD/SCID/IL2rγ^{null} newborn system provides a valuable tool to reproduce human hemato-lymphoid development.

Materials and methods

Mice

NOD.Cg-Prkdc^{scid}IL2rg^{tmlWjl}/Sz (NOD/SCID/IL2rγ^{null}) and NOD/LtSz-Prkdc^{scid}/B2m^{null} (NOD/SCID/β2m^{null}) mice were developed at the Jackson Laboratory (Bar Harbor, ME). The NOD/SCID/IL2rγ^{null} strain was established by backcrossing a complete null mutation at γc locus[16] onto the NOD.Cg-Prkdc^{scid} strain. The establishment of this mouse line has been reported elsewhere.[26] All experiments were performed according to the guideline in the Institutional Animal Committee of Kyushu University.

Cell preparation and transplantation

CB cells were obtained from Fukuoka Red Cross Blood Center (Japan). CB cells were harvested after written informed consent. Mononuclear cells were depleted of Lin$^+$ cells using mouse anti-hCD3, anti-hCD4, anti-hCD8, anti-hCD11b, anti-hCD19, anti-hCD20, anti-hCD56, and anti–human glycophorin A (hGPA) monoclonal antibodies (BD Immunocytometry, San

Jose, CA). Samples were enriched for hCD34$^+$ cells by using anti-hCD34 microbeads (Miltenyi Biotec, Auburn, CA). These cells were further stained with anti-hCD34 and hCD38 antibodies (BD Immunocytometry), and were purified for Lin$^-$CD34$^+$CD38$^-$ HSCs by a FACSVantage (Becton Dickinson, San Jose, CA). Lin$^-$ hCD34$^+$ cells (10^5) or 2 × 10^4 Lin$^-$hCD34$^+$hCD38$^-$ cells were transplanted into irradiated (100 cGy) NOD/SCID/IL2rγ^{null} or NOD/SCID/β2m^{null} newborns via a facial vein[27] within 48 hours of birth.

Examination of hematopoietic chimerism

At 3 months after transplantation, samples of peripheral blood, bone marrow, spleen, and thymus were harvested from recipient mice. Human common lymphoid progenitors were analyzed based on the expression of hCD127 (IL-7 receptor α chain) and hCD10 in Lin (hCD3, hCD4, hCD8, hCD11b, hCD19, hCD20, hCD56, and hGPA)$^-$ hCD34$^+$hCD38$^+$ fraction.[28,29] Human myeloid progenitors were analyzed based on the expressions of hCD45RA and hCD123 (IL-3 receptor α chain) in Lin$^-$ CD10$^-$CD34$^+$CD38$^+$ fractions. For the analysis of megakaryocyte/ erythroid (MegE) lineages, anti-hCD41a (HIP8), anti-hGPA (GAR-2), anti-mCD41a (MW Reg30), and anti-mTer119 (Ter-119) antibodies were used. Samples were treated with ammonium chloride to eliminate mature erythrocytes, and were analyzed by setting nucleated cell scatter gates. For the analysis of circulating erythrocytes and platelets, untreated blood samples were analyzed by setting scatter gates specific for each cell fraction. Human B lymphoid progenitors were evaluated according to the criteria proposed by LeBien.[30]

Methylcellulose culture assay

Bone marrow cells of recipient mice were stained with anti-hCD34, hCD38, hCD45RO, hCD123, and lineage antibodies. Human HSCs, CMPs, GMPs, and MEPs were purified according to the phenotypic definition[28,29] by using a FACSVantage (Becton Dickinson). One hundred cells of each population were cultured in methylcellulose media (Stem Cell Technologies, Vancouver, BC, Canada) supplemented with 10% bovine serum albumin (BSA), 20 μg/mL steel factor, 20 ng/mL IL-3, 20 ng/mL IL-11, 20 ng/mL Fms-like tyrosine kinase 3 (Flt3) ligand, 50 ng/mL granulocyte-macrophage colony-stimulating factor (GM-CSF), 4 U/ml erythropoietin (Epo), and 50 ng/mL thrombopoietin (Tpo). Colony numbers were enumerated on day 14 of culture.

Histologic analysis

Tissue samples were fixed with 4% paraformaldehyde and dehydrated with graded alcohol. After treatment with heated citrate buffer for antigen retrieval, paraformaldehyde-fixed paraffin-embedded sections were immunostained with mouse anti-hCD19, anti–human IgA, anti-hCD3, anti-hCD4, anti-hCD8, and anti-hCD11c antibodies (Dako Cytomation, Carpinteria, CA). Stained specimens were observed by confocal microscopy (LSM510 META microscope; Carl Zeiss, Oberkochen, Germany). Image acquisition and data analysis were performed by using LSM5 software. Numerical aperture of the objective lens (PlanApochromat ×63) used was 1.4.

ELISA

Human Ig concentration in recipient sera was measured by using a human immunoglobulin assay kit (Bethyl, Montgomery, IL). For detection of ovalbumin (OVA)–specific human IgM and IgG antibodies, 5 recipient mice were immunized twice every 2 weeks with 100 μg of OVA (Sigma, St Louis, MO) that were emulsified in aluminum hydroxide (Sigma). Sera from OVA-treated mice were harvested 2 weeks after the second immunization. OVA was plated at s concentration of 20 μg/mL on 96-microtiter wells at 4°C overnight. After washing and blocking with bovine serum albumin, serum samples were incubated in the plate for 1 hour. Antibodies binding OVA were then measured by a standard enzyme-linked immunosorbent assay (ELISA).

Cytotoxicity of alloantigen-specific human CD4+ and CD8+ T-cell lines

Alloantigen-specific human CD4+ and CD8+ T-cell lines were established according to the method as reported.[31] After stimulation with an Epstein Barr virus–transformed B lymphoblastoid cell line (TAK-LCL) established from a healthy individual (TAK-LCL) for 6 days, 100 hCD4+ T cells or hCD8+ T cells were plated with 3×10^4 TAK-LCL cells in the presence of 10 U/mL human IL-2 (Genzyme, Boston, MA), and were subjected to a chromium 51 (^{51}Cr) release assay. A Limiting number of effector cells and 10^4 ^{51}Cr-labeled allogeneic target cells were incubated. KIN-LCLs that do not share HLA with effector cells or TAK-LCL were used as negative controls. Cytotoxic activity was tested in the presence or absence of anti-HLA class I or anti–HLA-DR monoclonal antibodies.

Results

Reconstitution of human hematopoiesis is achieved in NOD/SCID/IL2rγ null mice

NOD/SCID/IL2rγ[null] mice lacked mature murine T or B cells evaluated by fluorescence-activated cell sorting (FACS), and displayed extremely low levels of NK cell activity.[31] This mouse line can survive more than 15 months[31] since it does not develop thymic lymphoma, usually a fatal disease in the immune-compromised mice with NOD background.[32]

Lin−hCD34+ CB cells contain HSCs, and myeloid and lymphoid progenitors.[28,29] We and others have reported that engraftment of human CB cells, which contain hematopoietic stem and progenitor cells, was efficient in NOD/SCID/$\beta 2m^{-/-}$ and RAG2$^{-/-}$/$\gamma_c^{-/-}$ mice, especially when cells were transplanted during the neonatal period.[14,33] We therefore transplanted purified Lin−hCD34+ CB cells into sublethally irradiated NOD/SCID/IL2rγ[null] newborns via a facial vein.[27]

We first transplanted 10^5 Lin−hCD34+ CB cells from 3 independent donors into 5 NOD/SCID/IL2rγ[null] newborns, and found that the NOD/SCID/IL2rγ[null] newborn system is very efficient for supporting engraftment of human hematopoietic progenitor cells. Table 1 shows percentages of hCD45+ cells in these mice 3 months after transplantation. Strikingly, the average

Table 1. Chimerism of human CD45+ cells in NOD/SCID/β2m null mice and NOD/SCID/IL2rγ null mice

Mouse no. (donor no.)	% nucleated cells		
	PB	BM	Spleen
NOD/SCID/IL2rγ null			
1 (1)	71.2	70.9	66.8
2 (1)	81.7	81.4	47.1
3 (2)	50.1	58.8	49.5
4 (3)	68.0	83.1	51.1
5 (3)	73.3	70.1	58.1
Mean ± SD	68.9 ± 11.6*	72.9 ± 9.8*	54.5 ± 8.0*
NOD/SCID/β2m null			
1 (1)	10.4	46.1	22.0
2 (2)	11.6	31.5	24.3
3 (3)	6.9	18.1	20.7
4 (3)	20.7	30.4	31.2
Mean ± SD	12.4 ± 5.9*	31.5 ± 11.5*	22.6 ± 4.7*

To compare the engraftment levels in the two strains, 1×10^5 Lin− CD34+ cells derived from 3 CB samples were transplanted into 5 NOD/SCID/IL2rγ[null] mice and 4 NOD/SCID/β2m[null] mice. At 3 months after transplantation, BM, spleen, and peripheral blood (PB) of the recipient mice were analyzed for the engraftment of human cells. Data show percentages of human CD45+ cells in each tissue.

*$P < .05$.

engraftment levels were approximately 70% in both the bone marrow and the peripheral blood. Compared with 4 control NOD/SCID/$\beta 2m^{-/-}$ recipient mice given transplants from the same donors, engraftment levels of hCD45+ cells in NOD/SCID/IL2rγ[null] mice were significantly higher (Table 1).

Table 2 shows the analysis of human hematopoietic cell progeny in mice that received transplants of human Lin−hCD34+ CB cells. In the peripheral blood, hCD45+ cells included hCD33+ myeloid, hCD19+ B cells, and hCD3+ T cells in all mice analyzed (Figure 1A and Table 2). We then analyzed the reconstitution of erythropoiesis and thrombopoiesis in these mice. Anti–human glycophorin A (hGPA) antibodies recognized human erythrocytes, while mTer119 antibodies[34] recognized GPA-associated protein on murine erythrocytes, respectively (Figure 1B). Human and murine platelets could also be stained with anti–human and anti–murine CD41a, respectively (Figure 1B). Circulating hGPA+ erythrocytes and hCD41a+ platelets were detected in all 3 mice analyzed (Figure 1B, right panels). hGPA+ erythroblasts and hCD41a+ megakaryocytes were detected as 9.5% ± 6.2% (n = 5) and 1.64% ± 0.42% (n = 5) of nucleated bone marrow cells, respectively. Thus, transplanted human Lin−hCD34+ CB cells differentiated into mature erythrocytes and platelets in NOD/SCID/IL2rγ[null] recipients.

In all engrafted mice, the bone marrow and the spleen contained significant numbers of hCD11c+ dendritic cells as well as hCD33+ myeloid cells, hCD19+ B cells, and hCD3+ T cells (Table 2 and Figure 1C). hCD11c+ dendritic cells coexpressed HLA-DR that is essential for antigen presentation to T cells (Figure 1D). In contrast, in the thymus, the majority of cells were composed of hCD3+ T cells and rare hCD19+ B cells (Table 2).

Figure 2A shows the change in the percentage of circulating hCD45+ cells in another set of NOD/SCID/IL2rγ[null] newborns injected with 2×10^4 Lin−hCD34+hCD38− CB cells. Surprisingly, the level of hCD45+ cells in the blood was unchanged, and was maintained at a high level even 24 weeks after transplantation. Mice did not develop lymphoid malignancies or other complications. Furthermore, we tested the retransplantability of human HSCs in primary recipients. We killed mice at 24 weeks after the primary transplantation of hCD34+ cells, purified 1 to 5×10^4 hCD34+ cells from primary recipient bone marrow cells, and retransplanted them into NOD/SCID/IL2rγ[null] newborns. In all 3 experiments, secondary recipients successfully reconstituted human hematopoiesis at least until 12 weeks after transplantation, when we killed mice for the bone marrow analysis (Figure 2B). Thus, the NOD/SCID/IL2rγ[null] newborn system can support human hematopoiesis for the long term.

Human cord blood hematopoietic stem cells produced myeloid and lymphoid cells via developmental intermediates in the NOD/SCID/IL2rγ null bone marrow

The Lin−hCD34+ CB fraction contains early myeloid and lymphoid progenitors as well as HSCs.[28] To verify that differentiation into all hematopoietic cells can be initiated from human HSCs in the NOD/SCID/IL2rγ[null] newborn system, we transplanted Lin−hCD34+hCD38−CB cells that contain the counterpart population of murine long-term HSCs,[35] and are highly enriched for human HSCs.[36,37] hCD34+ CB cells (15%-20%) were hCD38− (data not shown). Mice given transplants of 2×10^4 Lin−hCD34+hCD38− cells displayed successful reconstitution of similar proportion of human cells compared with mice reconstituted with 1×10^5 Lin−hCD34+ cells at 12 weeks after transplantation (Table 2). In another experiment, mice injected with 2×10^4 Lin−hCD34+hCD38− cells exhibited the high chimerism (> 50%)

Table 2. Cellular number and composition in tissues of engrafted NOD/SCID/IL2rγ^{null} mice

Injected cells, mice, and tissue type	Total no. cells	% nucleated cells (% hCD45+ cells)			
		CD33	CD19	CD3	CD11c
1 × 10^5 Lin$^-$CD34$^+$					
Mouse no. 1/ donor no. 1					
BM	2.4 × 10^7	8.2 (11.6)	54.8 (77.6)	10.7 (15.1)	1.1 (1.6)
Spleen	4.1 × 10^7	4.3 (6.4)	33.5 (50.1)	26.1 (39.1)	2.2 (3.3)
Thymus	3.1 × 10^5	NE	1.3 (1.3)	96.2 (98.7)	NE
PB	NE	4.0 (5.6)	35.1 (49.3)	19.8 (27.8)	NE
Mouse no. 2/donor no. 1					
BM	1.8 × 10^7	5.5 (6.8)	56.5 (67.6)	9.9 (12.2)	2.9 (3.6)
Spleen	3.2 × 10^7	2.1 (4.5)	27.7 (58.8)	15.9 (33.8)	1.3 (2.8)
Thymus	4.5 × 10^5	NE	1.1 (1.2)	90.4 (98.8)	NE
PB	NE	6.1 (7.5)	53.8 (65.9)	21.6 (40.1)	NE
Mouse no. 4/ donor no. 3					
BM	1.9 × 10^7	9.4 (11.3)	52.9 (63.7)	15.9 (19.1)	0.62 (0.75)
Spleen	4.4 × 10^7	3.5 (6.8)	24.2 (47.4)	20.8 (40.7)	1.5 (2.9)
Thymus	0.8 × 10^5	NE	0.88 (1.1)	78.2 (98.9)	NE
PB	NE	3.2 (4.7)	61.3 (90.1)	5.3 (7.8)	NE
Mouse no. 5/donor no. 3					
BM	2.1 × 10^7	10.2 (14.6)	48.8 (82.0)	9.4 (13.4)	1.3 (1.9)
Spleen	2.7 × 10^7	6.6 (11.4)	30.4 (52.3)	18.6 (32.0)	1.1 (1.9)
Thymus	1.1 × 10^5	NE	3.1 (3.7)	81.1 (96.3)	NE
PB	NE	9.8 (13.4)	40.4 (55.1)	16.8 (22.9)	NE
2 × 10^4 Lin$^-$CD34$^+$CD38$^-$					
Mouse no. 6/donor no. 4					
BM	2.6 × 10^7	3.1 (5.3)	46.1 (78.7)	8.1 (13.8)	1.3 (2.2)
Spleen	3.9v10^7	1.3 (2.7)	40.2 (83.9)	5.9 (12.3)	0.54 (1.1)
Thymus	1.9 × 10^5	NE	2.1 (2.3)	89.4 (97.7)	NE
PB	NE	5.4 (12.4)	28.9 (66.3)	9.3 (21.3)	NE
Mouse no. 7/donor no. 5					
BM	1.4 × 10^7	7.2 (14.2)	39.6 (78.1)	3.1 (6.1)	0.82 (1.6)
Spleen	2.2 × 10^7	2.4 (5.1)	37.2 (79.3)	6.8 (14.5)	0.52 (1.1)
Thymus	1.3 × 10^5	NE	0.6 (0.7)	85.1 (99.2)	NE
PB	NE	2.3 (41.7)	49.3 (89.5)	3.5 (6.4)	NE
Mouse no. 8/donor no. 6					
BM	1.1 × 10^7	6.1 (11.7)	36.8 (70.6)	7.7 (14.8)	2.5 (4.8)
Spleen	2.9 × 10^7	2.9 (4.6)	33.8 (53.1)	24.6 (38.6)	2.4 (3.8)
Thymus	1.9 × 10^5	NE	1.1 (1.2)	94.1 (97.0)	NE
PB	NE	8.1 (11.9)	50.2 (73.5)	10.0 (14.6)	NE

BM, spleen, and thymus were harvested from engrafted NOD/SCID/IL2rγ^{null} mice at 3 months after transplantation. Total cell numbers in BM and thymus represent the cells harvested from 2 femurs for BM and those harvested from a hemilobe for thymus. Recipients 1, 2, 4, and 5 received transplants of 1 × 10^5 Lin$^-$CD34$^+$ cells. Recipients 6, 7, and 8 received transplants of 2 × 10^4 Lin$^-$CD34$^+$CD38$^-$ cells. NE indicates not examined.

of circulating human blood cells even 24 weeks after transplantation (not shown), suggesting the long-term engraftment of self-renewing human HSCs.

In all mice injected with Lin$^-$hCD34$^+$hCD38$^-$ cells, hGPA$^+$ erythroid cells and hCD41a$^+$ megakaryocytes were present (not shown). We then tested whether differentiation of Lin$^-$hCD34$^+$hCD38$^-$ HSCs in the NOD/SCID/IL2rγ^{null} mouse microenvironment can recapitulate normal developmental processes in the human bone marrow. We and others have reported that phenotypically separable myeloid and lymphoid progenitors are present in the steady-state normal bone marrow in both mice[38,39] and humans.[28,29] Figure 2C shows the representative FACS analysis data of recipient's bone marrow cells. In all 3 mice tested, the bone marrow contained the hCD34$^+$hCD38$^-$ HSC[36,37] and the hCD34$^+$hCD38$^+$ progenitor fractions.[28] The hCD34$^+$hCD38$^+$hCD10$^+$hCD127 (IL-7Rα)$^+$ common lymphoid progenitor (CLP) population[29] was detected (Figure 2C, top panels). According to the phenotypic definition of human myeloid progenitors,[28] the hCD34$^+$hCD38$^+$ progenitor fraction was subfractionated into hCD45RA$^-$hCD123 (IL-3Rα)^{lo} common myeloid progenitor (CMP), hCD45RA$^-$hCD123$^-$ megakaryocyte/erythro-

cyte progenitor (MEP), and hCD45RA$^+$hCD123^{lo} granulocyte/monocyte progenitor (GMP) populations (Figure 2C, bottom panels). We then purified these myeloid progenitors, and tested their differentiation potential. As shown in Figure 2D, purified GMPs and MEPs generated granulocyte/monocyte (GM)– and megakaryocyte/erythrocyte (MegE)–related colonies, respectively, while CMPs as well as HSCs generated mixed colonies in addition to GM and MegE colonies. These data strongly suggest that hCD34$^+$hCD38$^-$ human HSCs differentiate into all myeloid and lymphoid lineages tracking normal developmental steps of the steady-state human hematopoiesis within the NOD/SCID/IL2rγ^{null} mouse bone marrow.

Development of human systemic and mucosal immune systems in NOD/SCID/IL2rγ^{null} mice

We further evaluated development of the human immune system in NOD/SCID/IL2rγ^{null} recipients. In the thymus, thymocytes were mostly consisted of hCD3$^+$ T cells with scattered hCD19$^+$ B cells (Figure 3A-B). This is reasonable since the normal murine thymus contain a small number of B cells in addition to T cells.[40]

Figure 1. Analysis of human hematopoietic cells in NOD/SCID/IL2rγ^null recipients. (A) In the scatter gates for nucleated cells, anti-hCD45 and anti-mCD45 antibodies (Abs) reacted exclusively with human and murine leukocytes, respectively. In the recipient blood, the majority of nucleated cells were human leukocytes (top row). High levels of engraftment by hCD33+ myelomonocytic cells, hCD19+ B cells, and hCD3+ T cells were achieved in peripheral blood of recipient mice given transplants of Lin−hCD34+ CB cells (bottom row). (B) Analysis of circulating erythrocytes (top row) or platelets (bottom row) in a NOD/SCID/IL2rγ^null recipient. In the blood, Ter119+ murine erythrocytes as well as hGPA+ human erythrocytes were detected. mCD41a+ murine platelets were also reconstituted. (C) Multilineage engraftment of human cells in the NOD/SCID/IL2rγ^null murine bone marrow. hCD33+ myelomonocytic cells, hCD19+ B cells, and hCD3+ T cells were present. hGPA+ erythroid cells and hCD41a+ megakaryocytes were also seen in the nucleated cell gate of the bone marrow. (D, left) HLA-DR+hCD11c+ dendritic cells were detected in the spleen by a flow cytometric analysis. (Right) Immunohistochemical staining of CD11c in the spleen. CD11c+ cells displayed dendritic cell morphology.
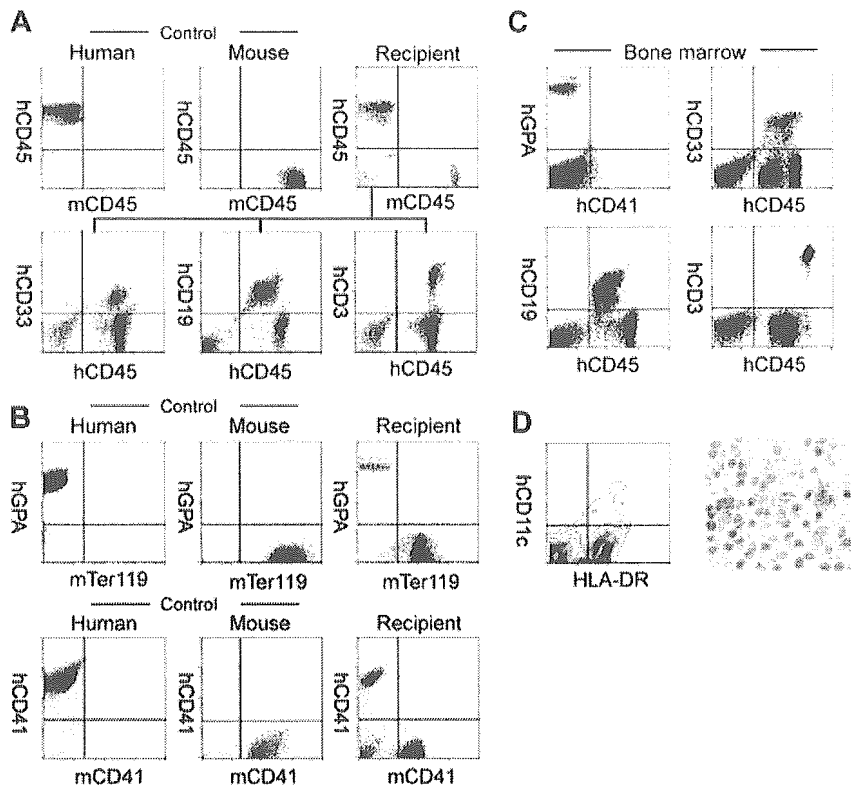

Thymocytes consisted of immature hCD4+hCD8+ double-positive (DP) T cells (Figure 3C) as well as small numbers of hCD4+ or hCD8+ single-positive (SP) mature T cells (Figure 4A, top panel), while hCD3+ human T cells in spleen were mainly constituted of either hCD4+ or hCD8+ single positive T cells (Figure 4A, bottom panel). These data suggest that normal selection processes of T-cell development may occur in the recipients' thymi.

In the spleen, lymphoid follicle-like structures were seen (Figure 3D-E), where predominant hCD19+ B cells were associated with surrounding scattered hCD3+ T cells (Figure 3F). Development of mesenteric lymph nodes was also observed, where the similar follicle-like structures consisted of human B and T cells were present (not shown). In the bone marrow and the spleen, nucleated cells in each organ contained hCD34+hCD19+ pro-B cells, hCD10+hCD19+ immature B cells, and hCD19+hCD20+ mature B cells (Figure 4B). Figure 4C shows the expression of human immunoglobulins on hCD19+ B cells. A significant fraction of hCD19+ B cells expressed human IgM on their surface. A
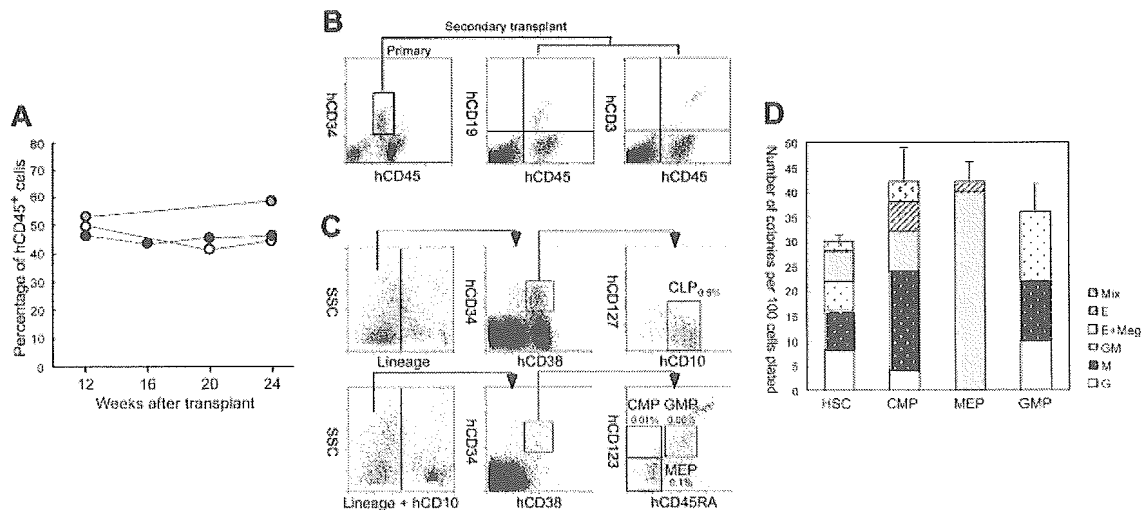
Figure 2. Purified Lin−hCD34+hCD38− CB cells reconstitute hematopoiesis via physiological intermediates, and display long-term reconstitution in the NOD/SCID/IL2rγ^null newborn system. (A) Serial evaluation of chimerism of human cells in peripheral blood of recipient mice injected with 2 × 10^4 Lin−hCD34+hCD38− CB cells. White, gray, and black dots represent 3 individual recipients. (B) hCD34+ cells purified from a primary recipient marrow (left) were successfully engrafted into the secondary newborn recipients. hCD19+ B cells (middle) and hCD3+ T cells (right) in a representative secondary recipient is shown. (C) The Lin− bone marrow cells contained hCD34+hCD38+hCD10+hCD127 (IL-7Rα)+ CLPs (top row). In the Lin−hCD10−fraction, hCD34+hCD38+hCD45RA−hCD123 (IL-3Rα)^lo CMPs, hCD34+hCD38+hCD45RA+hCD123^lo GMPs, hCD34+hCD38+hCD45RA−hCD123− MEPs were present. Each number for progenitors indicates percentages of hCD45+ cells. SSC indicates side scatter. (D) Colony-forming activity of purified myeloid progenitor population in the methylcellulose assay. Representative data from 1 of 3 recipients are shown. Error bars represent standard deviation.
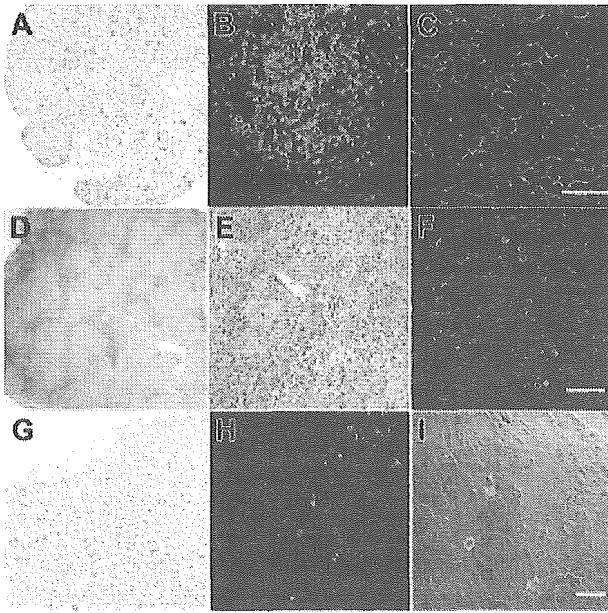
Figure 3. Histology of lymphoid organs in engrafted NOD/SCID/IL2rγ^null recipients. (A) The thymus showed an increased cellularity after reconstitution. (B) The thymus stained with anti-hCD3 (green) and anti-hCD19 (red) antibodies. (C) The thymus stained with anti-hCD4 (green) and anti-hCD8 (red) antibodies. The majority of thymocytes are doubly positive for hCD4 and hCD8. (D-E) Lymphoid follicle-like structures in the spleen of a recipient. (F) The lymphoid follicles mainly contained hCD19⁺ B cells (red) that were surrounded by scattered hCD3⁺ T cells (green). (G) Histology of the intestine in an engrafted NOD/SCID/IL2rγ^null recipient (left). (H) In the intestine, DAPI⁺ (4′,6-diamidino-2-phenylindole)–nucleated cells (blue) contained both scattered hCD3⁺ T cells (green) and human IgA⁺ cells (red). (I) The DIC image of the same section shows that IgA⁺ B cells were mainly found in the interstitial region of the intestinal mucosal layer. White bars inside panels represent 80 μm (C), 100μm (F), and 20μm (I).

fraction of cells expressing IgD were also observed in the blood and the spleen, suggesting that class switching occurred in these developing B cells. As reported in the Rag2$^{-/-}$ γc$^{-/-}$ mouse models,[10,12,14] hCD19⁺IgA⁺ B cells were detected in the bone marrow and the spleen in NOD/SCID/IL2rγ^null recipients. We then evaluated concentrations of human immunoglobulins in sera of mice given transplants of human Lin⁻hCD34⁺ CB cells by ELISA. In all sera from 3 NOD/SCID/IL2rγ^null recipients, a significant amount of IgG (257 ± 76 μg/mL) and IgM (600 ± 197 μg/mL) were detectable, whereas sera from the control NOD/SCID/β2m$^{-/-}$ mice contained lower levels of IgM (76 ± 41 μg/mL) and little or no IgG (Table S1, available on the *Blood* website; see the Supplemental Table link at the top of the online article). These data collectively suggest that class-switching can effectively occur in NOD/SCID/IL2rγ^null mice.

The intestinal tract is one of the major sites for supporting host defense against exogenous antigens. Since bone marrow and spleen hCD19⁺ B cells contained a significant fraction of cells expressing IgA, we tested whether reconstitution of mucosal immunity could be achieved in the NOD/SCID/IL2rγ^null recipients. Immunohistologic analyses demonstrated that the intestinal tract of recipient mice contained significant numbers of cells expressing human IgA in addition to hCD3⁺ T cells (Figure 3G-I). Thus, human CB cells could reconstitute cells responsible for both systemic and mucosal immunity in the NOD/SCID/IL2rγ^null newborn system.

Function of adaptive human immunity in engrafted NOD/SCID/IL2rγ^null mice

Five NOD/SCID/IL2rγ^null mice reconstituted with 3 independent human CB samples were immunized twice with ovalbumin (OVA)

at 3 months after transplantation. Two weeks after immunization, sera were collected from these immunized mice, and were subjected to ELISA to quantify OVA-specific human IgG and IgM. As shown in Figure 5A, significant levels of OVA-specific human IgM and IgG were detected in all serum samples from immunized mice, but not in samples from nonimmunized engrafted mice. Thus, the adaptive human immune system properly functioned in the NOD/SCID/IL2rγ^null strain to produce antigen-specific human IgM and IgG antibodies.

We next tested the alloantigen-specific cytotoxic function of human T cells developed in NOD/SCID/IL2rγ^null recipients. hCD3⁺ T cells isolated from the spleen of NOD/SCID/IL2rγ^null recipients were cultured with allogeneic B-LCL (TAK-LCL). We established 8 hCD4⁺ and 10 hCD8⁺ T-cell clones responding LCL-specific allogeneic antigens. We then estimated cytotoxic activity of these T-cell clones in the presence or absence of anti–HLA-DR and anti–HLA class I antibodies. We randomly chose 3 each of CD4 and CD8 clones for further analysis (Figure 5B). A ^{51}Cr release assay revealed that both hCD4⁺ and hCD8⁺ T cell clones exhibited cytotoxic activity against allogeneic TAK-LCL, whereas they showed no cytotoxicity against KIN-LCL, a cell line not sharing HLA classes I or II with TAK-LCL. Cytotoxic activity of hCD4⁺
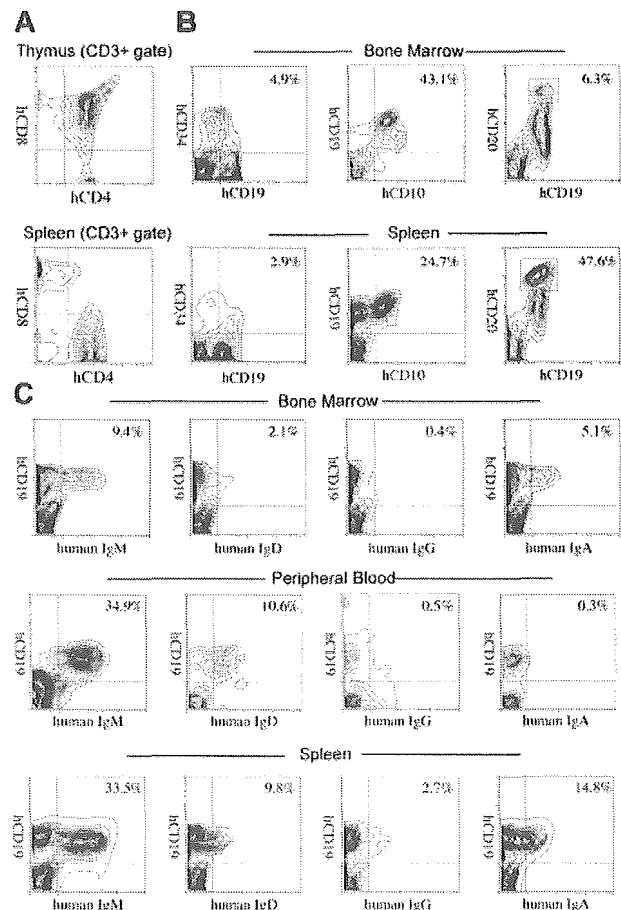
Figure 4. Development of lymphocytes in NOD/SCID/IL2rγ^null recipients. (A) The flow cytometric analysis of human T cells in recipients. The majority of cells in the thymus were hCD4⁺hCD8⁺ double-positive thymocytes (top). The CD3⁺ spleen cells contained hCD4⁺ or hCD8⁺ single-positive mature T cells (bottom). (B) hCD34⁺hCD19⁺ pro-B, hCD10⁺hCD19⁺ pre-B, and hCD19⁺hCD20^hi mature B cells were seen in different proportions in the bone marrow and the spleen of recipient mice. Numbers represent percentages within total nucleated cells. (C) B cells expressing each class of human immunoglobulin heavy chain were seen in the bone marrow, the peripheral blood (PB), or the spleen of engrafted NOD/SCID/IL2rγ^null mice. Numbers represent percentages out of nucleated cells.

Figure 5. Functional analysis of human T and B cells developed in NOD/SCID/IL2rγ^{null} recipients. (A) Production of OVA-specific human immunogloblins. Two weeks after immunization with OVA, sera of 5 independent recipients were sampled, and were evaluated for the concentration of OVA-specific human IgM (□) and IgG (▣) by ELISA. Sera of 3 nonimmunized NOD/SCID/IL2rγ^{null} recipients were used as controls. O.D. indicates optical density. (B) Cytotoxic activity of human T cells generated in NOD/SCID/IL2rg-null mice. hCD4$^+$ and hCD8$^+$ T-cell clones derived from the recipient spleen were cocultured with allogeneic target cells (TAK-LCLs). KIN-LCLs that do not share any HLA type with effector cells or TAK-LCLs (X) were used as negative controls. Both hCD4$^+$ and hCD8$^+$ T-cell lines displayed cytotoxic activity against TAK-LCL in a dose-dependent manner. In hCD4$^+$ T-cell clones, this effect was blocked by anti-HLA-DR antibodies (▲), whereas in hCD8$^+$ T-cell clones, the effect was blocked by anti-HLA class I antibodies (■). ◆ indicates cytotoxic response to TAK-LCLs without addition of antibodies.
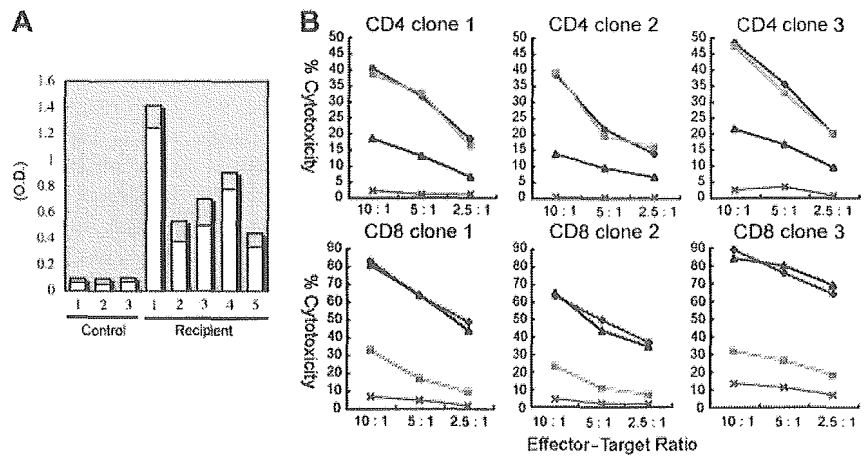
and hCD8$^+$ T cell clones was significantly inhibited by the addition of anti–HLA-DR and anti–HLA class I antibodies, respectively. These data clearly demonstrate that human CB-derived T cells can exhibit cytotoxic activity in an HLA-restricted manner.

Discussion

Xenogeneic transplantation models have been extensively used to study human hematopoiesis in vivo.[1,41,42] In the present study, we describe a new xenogeneic transplantation system that effectively supports human hemato-lymphoid development of all lineages for the long term.

NOD/SCID/IL2rγ^{null} newborns exhibited very efficient reconstitution of human hematopoietic and immune systems after intravenous injection of a relatively small number of CB cells. In our hands, NOD/SCID/IL2rγ^{null} newborns displayed a significantly higher chimerism of human blood cells compared with NOD/SCID/β2m$^{-/-}$ newborns under an identical transplantation setting (Table 1). This result directly shows that the IL2rγ^{null} mutation has a merit on human cell engraftment over the β2m$^{-/-}$ mutation.

One of the critical problems in the NOD/SCID strain for the use of recipients is that this mouse line possesses a predisposition to thymic lymphoma due to an endogenous ectropic provirus (Emv-30).[32] Because of this, NOD/SCID and NOD/SCID/β2m$^{-/-}$ mice have the short mean lifespan of 8.5 and 6 months, respectively, while NOD/SCID/IL2rγ^{null} mice did not develop thymic lymphoma surviving more than 15 months,[31] which allows a long-term experimentation.

In our study, NOD/SCID/IL2rγ^{null} newborns injected with 10^5 hCD34$^+$ CB cells via a facial vein consistently displayed high levels of chimerism of human hematopoiesis (50%-80%; Table 1). This model is comparable to, or may be more efficient than the Rag2$^{-/-}$ γc$^{-/-}$ newborn model where intrahepatic injection of 0.4 to 1.2×10^5 hCD34$^+$ CB cells generated variable levels of chimerism of human cells (5%-65%).[14] This slight difference of engraftment efficiency, however, could reflect the homing efficiency of HSCs by each injection route. The NOD/SCID/IL2rγ^{null} newborn model might be more efficient than the NOD/SCID/γc$^{-/-}$ adult model in which the majority of recipients showed approximately 30% chimerism of human cells after transplantation of 5×10^4 hCD34$^+$ CB cells.[11] Although we did not test NOD/SCID/γc$^{-/-}$ newborns side by side in this study, we have found that the engraftment level of hCD34$^+$ cells of human acute myelogenous leukemia is approximately 3-fold higher in newborns than adults in

the NOD/SCID/IL2rγ^{null} strain (F.I., T.M., S.Y., M.Y., M.H., K.A., and L.D.S., manuscript in preparation). Therefore, it remains unclear whether the IL2rγ^{null} mutation has a significant advantage over the truncated γc mutation[11] for human cell engraftment. It is still possible that the improved engraftment efficiencies in the NOD/SCID/IL2rγ^{null} newborn system as compared to those in the NOD/SCID/γc$^{-/-}$ adult system reflect the age-dependent maturation of the xenogeneic barrier.

The Rag2$^{-/-}$ γc$^{-/-}$ newborn and NOD/SCID/γc$^{-/-}$ adult models have provided definitive evidences that functional T cells, B cells, and dendritic cells can develop from hematopoietic progenitor cells in immunodeficient mice. Class-switching of immunoglobulin in CB-derived B cells properly occurred in the NOD/SCID/IL2rγ^{null} but not in the NOD/SCID/β2m$^{-/-}$ newborns (Table S1), further confirming the advantage of the NOD/SCID/IL2rγ^{null} model. We also showed that, consistent with a previous report using the Rag2$^{-/-}$ γc$^{-/-}$ model,[14] human T and B cells developed in NOD/SCID/IL2rγ^{null} mice are capable of mounting antigen-specific immune responses. Interestingly, human T and B cells migrated into murine lymphoid organs and into the intestinal tissues to collaborate in forming lymphoid organ structures. Furthermore, we found that IgA-secreting human B cells can develop in the murine intestine, suggesting that human mucosal immunity could be generated. Thus, the cellular interaction and the lymphocyte homing could occur at least to some extent across the xenogenic barrier in this model. It is also of interest that developing human cells in the thymus displayed normal distribution of SP and DP cells (Figure 4A), and that mature human T cells displayed cytotoxic functions in an HLA-dependent manner (Figure 5B). This suggests that positive and/or negative selection of human T cells could occur in NOD/SCID/IL2rγ^{null} recipients. Thymic epithelial cells in recipients reacted with anti-murine but not anti-human centromere probes in a FISH assay (F.I. and M.H., unpublished data, September 2004), confirming their recipient's origin. Thus, it remains unclear how these human T cells effectively educated and developed in murine thymus. It is also possible that human mature T cells developed by extrathymic education and selection.

Our data directly show that the most primitive hCD34$^+$hCD38$^-$ CB cells are capable of generating the human myeloerythroid system in addition to the immune system in the NOD/SCID/IL2rγ^{null} recipients. The emergence of circulating hCD33$^+$ myelomonocytic cells after transplantation of human CB cells has been reported in the NOD/SCID/β2m$^{-/-}$ newborn[33] and the NOD/SCID/γc$^{-/-}$ adult[11] systems. Development of human erythropoiesis, however, has not been obtained in previous models,

although it has been reported that NOD/SCID mice can support terminal maturation of hCD71^{+} erythroblasts that were induced ex vivo from human HSCs by culturing with human cytokines.[43] We showed for the first time that human erythropoiesis and thrombopoiesis can develop in mice from primitive hCD34^{+}hCD38^{−} cells, as evidenced by the presence of erythroblasts and megakaryocytes in the bone marrow and of circulating erythrocytes and platelets in NOD/SCID/IL2rγ[null] recipients. It is important to note that the hCD34^{+}hCD38^{−} CB HSC population generated myeloid- and lymphoid-restricted progenitor populations such as CMPs, GMPs, MEPs, and CLPs in the bone marrow (Figure 2E-F). Thus, the NOD/SCID/IL2rγ[null] microenvironment might be able to support physiological steps of myelopoiesis and lymphopoiesis initiating from the primitive HSC stage.

In summary, we show that the NOD/SCID/IL2rγ[null] newborn system efficiently supports hemato-lymphoid development from primitive human HSCs, passing through physiological developmental intermediates. It also can support development of human systemic and mucosal immunity, and therefore may be useful to use

human immunity to produce immunoglobulins or experimental vaccines. The NOD/SCID/IL2rγ[null] newborn system might also serve as an efficient tool for understanding malignant hematopoiesis in humans, since the analysis of human leukemogenesis has mainly been dependent upon the NOD/SCID adult mouse system.[44-46] Our model might also be useful to reproduce the transforming process of human hematopoietic cells, as transplanted murine hematopoietic progenitor and stem cells can develop leukemia by transducing oncogenic fusion genes in syngeneic mouse models.[47,48] Thus, the use of this system should open a more efficient way to analyze normal and malignant human hematopoiesis.

Acknowledgments

References

1. Greiner DL, Hesselton RA, Shultz LD. SCID mouse models of human stem cell engraftment. Stem Cells. 1998;16:166-177.

2. McCune JM, Namikawa R, Kaneshima H, Shultz LD, Lieberman M, Weissman IL. The SCID-hu mouse: murine model for the analysis of human hematolymphoid differentiation and function. Science. 1988;241:1632-1639.

3. Mosier DE, Gulizia RJ, Baird SM, Wilson DB. Transfer of a functional human immune system to mice with severe combined immunodeficiency. Nature. 1988;335:256-259.

4. Kaneshima H, Namikawa R, McCune JM. Human hematolymphoid cells in SCID mice. Curr Opin Immunol. 1994;6:327-333.

5. Pflumio F, Izac B, Katz A, Shultz LD, Vainchenker W, Coulombel L. Phenotype and function of human hematopoietic cells engrafting immune-deficient CB17-severe combined immunodeficiency mice and nonobese diabetic-severe combined immunodeficiency mice after transplantation of human cord blood mononuclear cells. Blood. 1996;88:3731-3740.

6. Shultz LD, Lang PA, Christianson SW, et al. NOD/LtSz-Rag1null mice: an immunodeficient and radioresistant model for engraftment of human hematolymphoid cells, HIV infection, and adoptive transfer of NOD mouse diabetogenic T cells. J Immunol. 2000;164:2496-2507.

7. Goldman JP, Blundell MP, Lopes L, Kinnon C, Di Santo JP, Thrasher AJ. Enhanced human cell engraftment in mice deficient in RAG2 and the common cytokine receptor gamma chain. Br J Haematol. 1998;103:335-342.

8. Greiner DL, Shultz LD, Yates J, et al. Improved engraftment of human spleen cells in NOD/LtSz-scid/scid mice as compared with C.B-17-scid/scid mice. Am J Pathol. 1995;146:888-902.

9. Yoshino H, Ueda T, Kawahata M, et al. Natural killer cell depletion by anti-asialo GM1 antiserum treatment enhances human hematopoietic stem cell engraftment in NOD/Shi-scid mice. Bone Marrow Transplant. 2000;26:1211-1216.

10. Kollet O, Peled A, Byk T, et al. beta2 microglobulin-deficient (B2m(null)) NOD/SCID mice are excellent recipients for studying human stem cell function. Blood. 2000;95:3102-3105.

11. Ito M, Hiramatsu H, Kobayashi K, et al. NOD/SCID/gamma(c)(null) mouse: an excellent recipient mouse model for engraftment of human cells. Blood. 2002;100:3175-3182.

12. Hiramatsu H, Nishikomori R, Heike T, et al. Complete reconstitution of human lymphocytes from

cord blood CD34+ cells using the NOD/SCID/gammacnull mice model. Blood. 2003;102:873-880.

13. Leonard WJ. Cytokines and immunodeficiency diseases. Nat Rev Immunol. 2001;1:200-208.

14. Traggiai E, Chicha L, Mazzucchelli L, et al. Development of a human adaptive immune system in cord blood cell-transplanted mice. Science. 2004; 304:104-107.

15. Ohbo K, Suda T, Hashiyama M, et al. Modulation of hematopoiesis in mice with a truncated mutant of the interleukin-2 receptor gamma chain. Blood. 1996;87:956-967.

16. Cao X, Shores EW, Hu-Li J, et al. Defective lymphoid development in mice lacking expression of the common cytokine receptor gamma chain. Immunity. 1995;2:223-238.

17. DiSanto JP, Muller W, Guy-Grand D, Fischer A, Rajewsky K. Lymphoid development in mice with a targeted deletion of the interleukin 2 receptor gamma chain. Proc Natl Acad Sci U S A. 1995; 92:377-381.

18. Asao H, Takeshita T, Ishii N, Kumaki S, Nakamura M, Sugamura K. Reconstitution of functional interleukin 2 receptor complexes on fibroblastoid cells: involvement of the cytoplasmic domain of the gamma chain in two distinct signaling pathways. Proc Natl Acad Sci U S A. 1993;90: 4127-4131.

19. Takeshita T, Asao H, Ohtani K, et al. Cloning of the gamma chain of the human IL-2 receptor. Science. 1992;257:379-382.

20. Russell SM, Keegan AD, Harada N, et al. Interleukin-2 receptor gamma chain: a functional component of the interleukin-4 receptor. Science. 1993;262:1880-1883.

21. Noguchi M, Nakamura Y, Russell SM, et al. Interleukin-2 receptor gamma chain: a functional component of the interleukin-7 receptor. Science. 1993;262:1877-1880.

22. Kondo M, Takeshita T, Higuchi M, et al. Functional participation of the IL-2 receptor gamma chain in IL-7 receptor complexes. Science. 1994; 263:1453-1454.

23. Kondo M, Takeshita T, Ishii N, et al. Sharing of the interleukin-2 (IL-2) receptor gamma chain between receptors for IL-2 and IL-4. Science. 1993; 262:1874-1877.

24. Ferrag F, Pezet A, Chiarenza A, et al. Homodimerization of IL-2 receptor beta chain is necessary and sufficient to activate Jak2 and downstream signaling pathways. FEBS Lett. 1998;421: 32-36.

25. Reichel M, Nelson BH, Greenberg PD, Rothman PB. The IL-4 receptor alpha-chain cytoplasmic domain is sufficient for activation of JAK-1 and STAT6 and the induction of IL-4-specific gene expression. J Immunol. 1997;158:5860-5867.

26. Shultz LD, Lyons BL, Burzenski LM, et al. Human lymphoid and myeloid cell development in NOD/LtSz-scid IL2rgnull mice engrafted with mobilized human hematopoietic stem cells. J Immunol. 2005;174:6477-6489.

27. Sands MS, Barker JE, Vogler C, et al. Treatment of murine mucopolysaccharidosis type VII by syngeneic bone marrow transplantation in neonates. Lab Invest. 1993;68:676-686.

28. Manz MG, Miyamoto T, Akashi K, Weissman IL. Prospective isolation of human clonogenic common myeloid progenitors. Proc Natl Acad Sci U S A. 2002;99:11872-11877.

29. Galy A, Travis M, Cen D, Chen B. Human T, B, natural killer, and dendritic cells arise from a common bone marrow progenitor cell subset. Immunity. 1995;3:459-473.

30. LeBien TW. Fates of human B-cell precursors. Blood. 2000;96:9-23.

31. Yanai F, Ishii E, Kojima K, et al. Essential roles of perforin in antigen-specific cytotoxicity mediated by human CD4+ T lymphocytes: analysis using the combination of hereditary perforin-deficient effector cells and Fas-deficient target cells. J Immunol. 2003;170:2205-2213.

32. Prochazka M, Gaskins HR, Shultz LD, Leiter EH. The nonobese diabetic scid mouse: model for spontaneous thymomagenesis associated with immunodeficiency. Proc Natl Acad Sci U S A. 1992;89:3290-3294.

33. Ishikawa F, Livingston AG, Wingard JR, Nishikawa S, Ogawa M. An assay for long-term engrafting human hematopoietic cells based on newborn NOD/SCID/beta2-microglobulin(null) mice. Exp Hematol. 2002;30:488-494.

34. Kina T, Ikuta K, Takayama E, et al. The monoclonal antibody TER-119 recognizes a molecule associated with glycophorin A and specifically marks the late stages of murine erythroid lineage. Br J Haematol. 2000;109:280-287.

35. Okuno Y, Iwasaki H, Huettner CS, et al. Differential regulation of the human and murine CD34 genes in hematopoietic stem cells. Proc Natl Acad Sci U S A. 2002;99:6246-6251.

36. Craig W, Kay R, Cutler RL, Lansdorp PM. Expression of Thy-1 on human hematopoietic progenitor cells. J Exp Med. Vol. 177; 1993:1331-1342.

37. Terstappen LW, Huang S, Safford M, Lansdorp

PM, Loken MR. Sequential generations of hema-topoietic colonies derived from single nonlineage-committed CD34+CD38- progenitor cells. Blood. 1991;77:1218-1227.

38. Akashi K, Traver D, Miyamoto T, Weissman IL. A clonogenic common myeloid progenitor that gives rise to all myeloid lineages. Nature. 2000;404: 193-197.

39. Kondo M, Weissman IL, Akashi K. Identification of clonogenic common lymphoid progenitors in mouse bone marrow. Cell. 1997;91:661-672.

40. Akashi K, Richie LI, Miyamoto T, Carr WH, Weiss-man IL. B lymphopoiesis in the thymus. J Immu-nol. 2000;164:5221-5226.

41. Zanjani ED. The human sheep xenograft model for the study of the in vivo potential of human

HSC and in utero gene transfer. Stem Cells. 2000;18:151.

42. Stier S, Cheng T, Forkert R, et al. Ex vivo target-ing of p21Cip1/Waf1 permits relative expansion of human hematopoietic stem cells. Blood. 2003; 102:1260-1266.

43. Neildez-Nguyen TM, Wajcman H, Marden MC, et al. Human erythroid cells produced ex vivo at large scale differentiate into red blood cells in vivo. Nat Biotechnol. 2002;20:467-472.

44. Lumkul R, Gorin NC, Malehorn MT, et al. Human AML cells in NOD/SCID mice: engraftment poten-tial and gene expression. Leukemia. 2002;16: 1818-1826.

45. Hope KJ, Jin L, Dick JE. Acute myeloid leukemia originates from a hierarchy of leukemic stem cell

classes that differ in self-renewal capacity. Nat Immunol. 2004;5:738-743.

46. Bonnet D, Dick JE. Human acute myeloid leuke-mia is organized as a hierarchy that originates from a primitive hematopoietic cell. Nat Med. 1997;3:730-737.

47. Cozzio A, Passegue E, Ayton PM, Karsunky H, Cleary ML, Weissman IL. Similar MLL-associated leukemias arising from self-renewing stem cells and short-lived myeloid progenitors. Genes Dev. 2003;17:3029-3035.

48. Huntly BJ, Shigematsu H, Deguchi K, et al. MOZ-TIF2, but not BCR-ABL, confers proper-ties of leukemic stem cells to committed murine hematopoietic progenitors. Cancer Cell. 2004; 6:587-596.

ORIGINAL ARTICLE

Population pharmacokinetics of intravenous busulfan in patients undergoing hematopoietic stem cell transplantation

H Takama[1], H Tanaka[1], D Nakashima[1], R Ueda[2] and Y Takaue[3]

[1]Product Development Department, Pharmaceutical Division, Kirin Brewery Company Ltd, Shibuya-ku, Tokyo, Japan; [2]Department of International Medicine and Molecular Science, Nagoya City University Graduate School of Medical Science, Mizuho-ku, Nagoya, Aichi, Japan and [3]Hematopoetic Stem Cell Transplantation Unit, National Cancer Center Hospital, Chuo-ku, Tokyo, Japan

A population pharmacokinetic analysis was performed in 30 patients who received an intravenous busulfan and cyclophosphamide regimen before hematopoietic stem cell transplantation. Each patient received 0.8 mg/kg as a 2 h infusion every 6 h for 16 doses. A total of 690 concentration measurements were analyzed using the nonlinear mixed effect model (NONMEM) program. A one-compartment model with an additive error model as an intraindividual variability including an interoccasion variability (IOV) in clearance (CL) was sufficient to describe the concentration–time profile of busulfan. Actual body weight (ABW) was found to be the determinant for CL and the volume of distribution (V) according to NONMEM analysis. In this limited study, the age (range 7–53 years old; median, 30 years old) had no significant effect on busulfan pharmacokinetics. For a patient weighting 60 kg, the typical CL and V were estimated to be 8.87 l/h and 33.8 l, respectively. The interindividual variability of CL and V were 13.6 and 6.3%, respectively. The IOV (6.6%) in CL was estimated to be less than the intraindividual variability. These results indicate high interpatient and intrapatient consistency of busulfan pharmacokinetics after intravenous administration, which may eliminate the requirement for pharmacokinetic monitoring.
Bone Marrow Transplantation (2006) **37**, 345–351.
doi:10.1038/sj.bmt.1705252; published online 9 January 2006
Keywords: intravenous; busulfan; population pharmacokinetics; NONMEM

Introduction

A high dose of busulfan in combination with cyclophosphamide is a widely used myeloablative conditioning

regimen before both allogenic and autologous bone marrow transplantation (BMT).[1,2] In most cases, busulfan is administered every 6-h over four consecutive days with a total standard dose of 16 mg/kg.[1] As with most alkylating agent, busulfan has a narrow therapeutic window. The dose-limiting toxicity of busulfan in the myeloablative conditioning regimen is hepatic veno-occlusive disease (VOD), which can lead to fatal liver failure.[3,4] Following administration of the oral formulation, very wide inter- and intraindividual systemic exposure has been reported,[5] which may be linked to erratic intestinal absorption, variable hepatic metabolism, circadian rhythm, genetics, diagnosis, drug–drug interaction and age.[5–9] Recently, the intravenous formulation of busulfan has been developed in order to minimize variations of the inter- and intrainidividual systemic exposure and to provide complete dose assurance. The intravenous busulfan is registered in the USA (Busulfex™) and in Europe (Busilvex™) for adults. The recommended dosage was 0.8 mg/kg/dose for 16 consecutive doses in adults.[10–12] There have been several reports about intravenous busulfan pharmacokinetics,[10–13] with only a few applying population pharmacokinetic analysis.[13] We report here, the results of the population pharmacokinetic modeling of intravenous busulfan. The aim of this analysis was to characterize the pharmacokinetics of intravenous busulfan, including the IOV and covariate relationships in patients.

Materials and methods

Patients

A total of 30 Japanese patients (27 adults and three children) receiving a first BMT entered in a Phase 2 study were investigated. These patients received busulfan at 0.8 mg/kg as a 2 h infusion every 6 h for four consecutive days. Following busulfan therapy, patients were given cyclophosphamide at 60 mg/kg as a 3 h infusion daily for 2 days. In order to prevent seizures, phenytoin (5–10 mg/kg/day) was administered orally for 8 days, starting 2 days before the start of busulfan therapy. The following demographic and physiopathological data were considered in the analysis: diagnosis, acute myeloid leukemia (13), acute lymphocytic leukemia (5), chronic

346

myelogenous leukemia (5), myelodysplastic syndrome (3), non-Hodgkin's lymphoma (4); gender, male (20), female (10); age, 7–53 years (median = 30 years); actual body weight (ABW), 18.5–82.7 kg (median = 64.1 kg); height, 111–180 cm (median = 165.5 cm); body mass index, 14.40–29.10 kg/m^2 (median = 22.65 kg/m^2); serum albumin, 3.5–4.8 g/dl (median = 4.3 g/dl); creatinine, 0.2–1.2 mg/dl (median = 0.7 mg/dl); serum alanine transaminase (ALT), 8.0–109.0 IU/l (median = 21.0 IU/l); history of hepatic disease, no (27), yes (3); concomitant antifungal treatment, no (7), yes (23); concomitant 5-HT$_3$ antiemetic treatment, no (16), yes (14). The study was approved by an independent Ethical Committee at each center. All patients provided written informed consent before enrollment.

Pharmacokinetic sampling and busulfan determination
Serial blood samples were drawn from each patient immediately before the first and ninth busulfan dose and then 0.25, 0.5, 0.75, 1.92, 2.25, 2.5, 3, 4, 5 and 6 h after the start of the first and ninth dose. The 13th dose sampling of each patient was made immediately before the infusion and at 1.92 h from the start of infusion, respectively. Plasma samples obtained by centrifugation were stored frozen until analysis. Busulfan was assayed by a validated gas chromatographic-mass selective detection (GC-MSD) assay technique.[14] The calibration curves were linear over concentrations ranging from 62.5 (quantification limit) to 2000 ng/ml. Samples with a concentration higher than 2000 ng/ml were diluted such that the concentration fell within the range of the calibration curve. Acceptance criteria for validating the analytical results of each run were as follows. Quality control (QC) samples in duplicate at three concentrations (125, 500, and 1500 ng/ml) were incorporated into each run. The results of the QC samples provided the basis for accepting or rejecting the run. At least four of six QC samples had to be within ±20% of their respective nominal values, and two of six QC samples (both at the same concentration) had also to be within the ±20% respective nominal value. The GC-MSD for pharmacokinetic investigation was performed at BML Inc. (Saitama, Japan). A total of 690 concentration measurements were available.

Population pharmacokinetic analysis and model validation
Data were analyzed using the nonlinear mixed effect model (NONMEM) program (version 5.0, Globomax LLC, Hanover, MD, USA). As the population pharmacokinetic model is used for prediction, it is important to develop a model with validation.[15] Owing to the limited number of patients in this study, external validation of the population pharmacokinetic model could not be applied; therefore, the model was evaluated using bootstrapping, one of the internal validation techniques.[15,16]

Population pharmacokinetic modeling steps were as follows: (1) a basic pharmacokinetic modeling using the NONMEM program and obtaining Bayesian individual parameter estimates, (2) validation of a basic model using the bootstrap resampling technique, (3) generalized additive modeling (GAM) for the selection of covariate candidates, (4) final pharmacokinetic modeling to determine

the covariate model, and (5) validation of the final model. The NONMEM program and PREDPP package were used throughout the analysis. The first-order conditional estimation with interaction method was used in all analysis processes because of the extensive sampling design in the study. Initial pharmacokinetic parameter estimates for NONMEM modeling were calculated using the mean data obtained from all the patients by WinNonlin (version 3.3, Pharsight Corp., Mountain View, CA, USA).

Step 1: basic pharmacokinetic modeling without bootstrapping. One-compartment structural model with constant rate infusion was fitted to the busulfan concentration–time data. Interindividual variability in clearance (CL) was modeled using an exponential error model, as follows:

$$CL_i = CL \cdot \exp(\eta_i),$$

where CL_i represents the hypothetical true CL for the ith individual, CL is the typical population value of CL and η is independent, identically distributed random variables with mean 0 and variance ω^2. Interindividual variability in volume of distribution (V) was similarly modeled.

Residual intraindividual variability was identically distributed and was modeled using the additive error, constant coefficient of variation (CCV) error or the combination of the additive and CCV error models. The additive error model is described by the following equation:

$$Cp_{ij} = Cp_{mij} + \varepsilon_{ij},$$

where Cp_{ij} is the ith measured concentration in the jth individual and Cp_{mij} is the ith concentration predicted by the model at the ith observation time for the jth individual. ε is independent random variable with mean zero and variance σ^2. The magnitude of residual intraindividual variability usually depends on measurement, dosing, sampling and model misspecification errors.

IOV was introduced into the model as previously proposed.[17] The following expression was used for CL

$$CL_{ij} = CL \cdot \exp(\eta_i + \kappa_{ij}),$$

where CL_{ij} represents the hypothetical true CL for the ith individual at occasion j, CL is the typical population value of CL and η and κ are independent, identically distributed random variables both with mean 0 and variance ω^2 and π^2, respectively. IOV in V was similarly modeled.

With the fixed and random effects chosen, empirical Bayes estimates of pharmacokinetic parameters were subsequently obtained using POSTHOC option within the NONMEM program. The choice of a basic population model was based on monitoring the Akaike's information criterion (AIC). The reliability of the model selection was checked by the analysis of residual and by the visual inspection of plots of predicted versus measured concentrations.

Step 2: validation of a basic model using the bootstrap resampling technique. Resampling the original data with replacements generated 100 bootstrap samples. The resampling unit comprises samples obtained from each

patient. The appropriate structural model that best describes the data from each sample was determined. This was performed to ensure that the model, which best described the bootstrap data was not different from the basic used for developing the population pharmacokinetic model in the subsequent step. In addition, density plots of each pharmacokinetic parameter estimate were used to examine the adequacy of the basic model.

Step 3: selection of covariate candidates. Exploratory data analysis was performed on the empirical Bayesian parameter estimates from step 2 and treated as data to examine the distribution, shapes and relationships between covariates and individual pharmacokinetic parameter estimates.

The data were subjected to a stepwise (single term addition/deletion) procedure using the GAM procedure in the Xpose program (version 3.1)[18] running on the S-PLUS statistical software package (version 6.0, Insightful Corp., Seattle, WA, USA). Each covariate was allowed to enter the model in any of several functional representations. AIC was used for model selection.[19] At each step, the model was changed by the addition or deletion of the covariate that results in the largest decrease in AIC. The search was stopped when AIC reached a minimum value.

Step 4: population model building using NONMEM. For each NONMEM analysis, the improvement in fit obtained upon the addition of a covariate selected from step 3 to the regression model was assessed by changes in the NONMEM objective function. Minimization of the NONMEM objective function, equal to twice the negative log-likelihood of the data, is equivalent to maximizing the probability of the data. The change in the objective function of the NONMEM value is approximately χ^2 distributed. A difference in the NONMEM objective function value of 3.84, associated with a P-value of less than 0.05, was considered statistically significant.

The construction of the regression model for each structural model parameter was performed in three steps using the original data set. Covariates were first screened individually. The full model was then defined as incorporating all significant covariates. Lastly, the final model was elaborated by backward elimination from the full model.

Step 5: validation of the final population pharmacokinetic model. Two hundred bootstrap samples were generated by resampling with replacements and used for the evaluation of the stability of the final model built in step 4. The final population pharmacokinetic model was fitted repeatedly to the 200 additional bootstrap samples. The mean parameter estimates obtained from these bootstrap replications were compared with those obtained from the original data set.

The area under the plasma concentration–time curve

The area under the plasma concentration–time curve (AUC) in each patient was calculated according to the linear trapezoidal rule using WinNonlin. The AUC at the steady state was calculated for the ninth dose from dosing interval (from zero to last sampling time). The AUC in one of 30 patients after the ninth administration was not calculated because the last sample at the ninth dose was collected after the start of the next dose.

Results

Determination of a basic pharmacokinetic model
Plasma concentration versus time curves are shown in Figure 1. Parameter estimates of various structural models are given in Table 1. The models including IOV gave lower AIC values than the models not including IOV. The Additive model, including IOV and the combination of the additive and CCV error models (the combination error model) including IOV gave similar AIC values. Analysis of residuals and plots of observed versus predicted concentrations were performed to check the reliability of the basic model selection. The residuals calculated in the additive model including IOV were not obviously different from those obtained in the combination error model including IOV (data not shown). The stability of these two models was examined in a subsequent step.

Stability of the basic model as assessed using the bootstrap resampling technique
One hundred bootstrap replicates were generated from the original data and used for the evaluation of the stability of
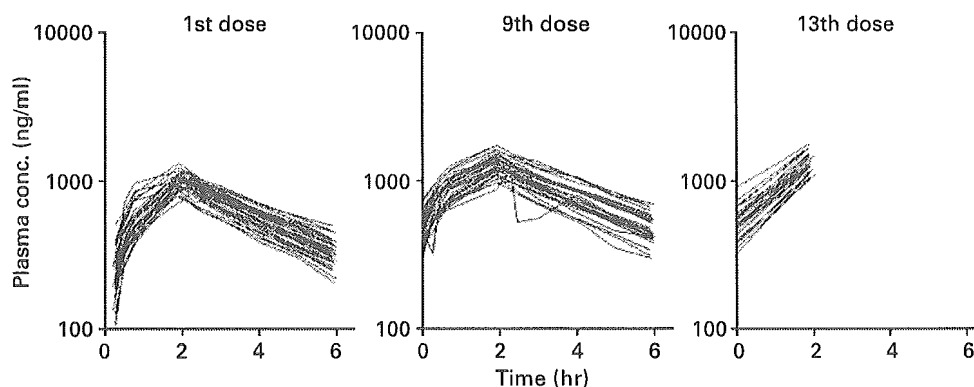
Figure 1 Observed plasma busulfan concentrations versus time.

Table 1 Parameter estimates of various models

Residual error	IOV	CL (l/h)	V (l)	AIC
CCV	No	8.56	28.9	7489
Additive	No	8.73	33.9	7235
Combination	No	8.73	33.8	7236
CCV	Yes	8.72	30.0	7421
Additive	Yes	8.77	33.4	7232
Combination	Yes	8.78	33.3	7233

IOV = interoccasion variability; CL = clearance; V = volume of distribution; AIC = akaike's information criterion; CCV = constant coefficient of variation model; additive = additive error model; combination = combination of the additive and CCV.

Table 2 Parameter estimates of the basic model

Parameter	Estimates
θ_{CL} (l/h)	8.77
θ_V (l)	33.4
ω_{CL} (%)	27.1
ω_V (%)	26.0
π_{CL} (%)	7.4
π_V (%)	1.4×10^{-3}
σ (ng/ml)	93.9

the basic pharmacokinetic model selected in the previous step. The parameter estimates could be obtained from all bootstrap data sets using the additive error model including IOV; however, one of 100 bootstrap data sets using the combination error model including IOV did not result in convergence. It was found that the additive model including IOV was more stable than the combination error model including IOV. Each parameter distribution of the additive error model including IOV is in a narrow range and almost unimodal (data not shown). Therefore, the additive error model including IOV was selected as the optimum basic model and was used in subsequent steps. Parameter estimates of the basic model are given in Table 2. As can be seen, the value of IOV in V is small, the decision was made whether the IOV introduces into V or not in subsequent steps. Plots of observed versus predicted concentration for the basic model are shown in Figure 2a.

Selection of covariate candidates
GAM analysis indicated that CL and V are functions of ABW (data not shown).

Population model building and stability of the final population models
The population model with covariates was built using the NONMEM program on the basis of the result of GAM analysis. ABW was found to be the predictor of both CL and V with a log-likelihood difference (LLD) of more than 10.83 ($P<0.001$) between each model in which ABW was introduced singly, and the basic model of each pharmacokinetic parameter modeled without ABW (data not shown). The full regression model was that following the allometric equations: $CL = \theta_1 \cdot (ABW/60)^{\theta_2}$, $V = \theta_3 \cdot (ABW/60)^{\theta_4}$, where θ_1 and θ_3 are the population values of CL and volume of distribution for the 60-kg patients. The IOV was not introduced into V in the population model since the IOV values obtained from each covariate model were negligible and the other parameter estimates were not changed by the introduction of IOV in V (data not shown). The full model was tested against the reduced models (Table 3).

The final population pharmacokinetic model obtained from the previous step was fitted repeatedly to the 200 bootstrapped samples. The parameter estimates of the final model using the original data and the mean parameter
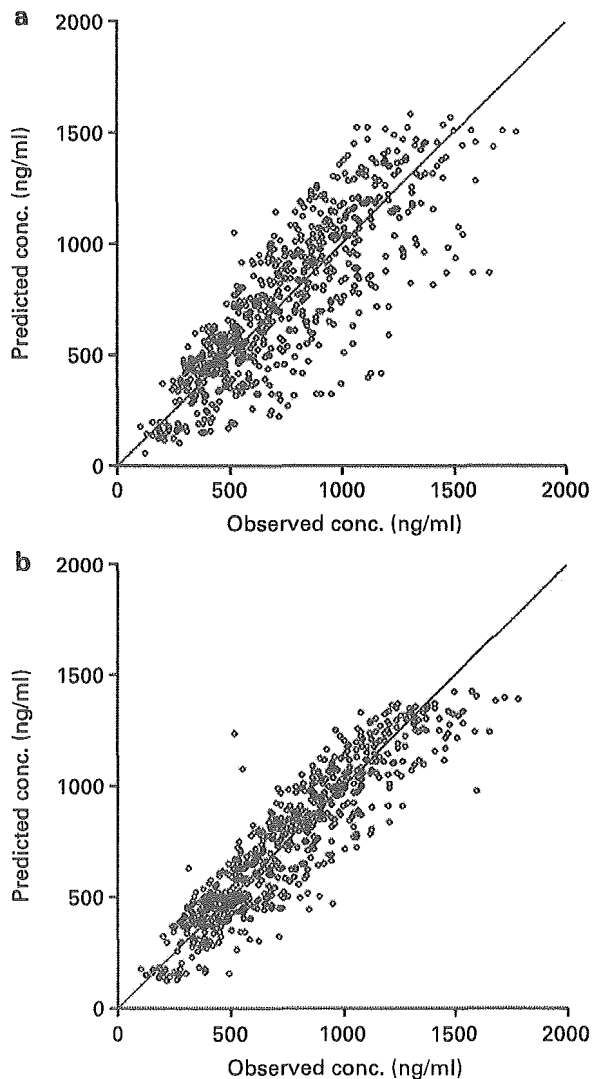
Figure 2 Plots of observed versus predicted concentration for the basic model (a) and for the final model (b).

estimates obtained from the 200 bootstrap replicates are provided in Table 4. The mean parameter estimates were within 15% of those obtained with the original data set. Plots of observed versus predicted concentrations for the final model are shown in Figure 2b. Plots of individual parameter values obtained from the model-independent technique versus ABW are shown in Figure 3. The final

Table 3 Comparison of the full and reduced model

Regression model	LLD (versus full model)
Full model	
$CL = \theta_1 \cdot (ABW/60)^{\theta 2}$	0
$V = \theta_3 \cdot (ABW/60)^{\theta 4}$	
Reduced model	
$\theta_2 = 0$	38.2*
$\theta_4 = 0$	64.9*

*$P < 0.001$.
LLD = log-likelihood difference.

Table 4 Typical population parameter estimates and stability of the final model

Parameters	Typical population parameter estimate (s.e.)[a]	Mean population parameter estimate (s.e.)[b]	Difference (%)[c]
$\theta_1{}^d$ (l/h)	8.87 (0.23)	8.86 (0.23)	−0.1
$\theta_2{}^d$	0.833 (0.077)	0.833 (0.103)	0.0
$\theta_3{}^e$ (l)	33.8 (0.6)	33.8 (0.7)	0.1
$\theta_4{}^e$	0.889 (0.049)	0.889 (0.060)	0.0
ω_{CL} (%)	13.6	13.2 (1.6)	−3.6
ω_V (%)	6.3	5.6 (2.3)	−12.3
π_{CL} (%)	6.6	6.1 (2.4)	−7.9
σ (ng/ml)	94.3	94.0 (8.3)	−0.3

[a]Obtained from the original data.
[b]Mean (s.e.) calculated from 200 bootstrap replicates.
[c](Bootstrap mean value-typical value from final model)/bootstrap mean value × 100(%).
[d]$CL = \theta_1 \cdot (ABW/60)^{\theta 2}$.
[e]$V = \theta_3 \cdot (ABW/60)^{\theta 4}$.

population model was well described the relationships between the pharmacokinetic parameters and ABW.

Discussion

The objective of population pharmacokinetic analysis was to characterize the pharmacokinetics of the intravenous busulfan including IOV and covariate relationships in patients. Reliability of results obtained from population analyses depends on the modeling procedure. Therefore, the evaluation of basic (covariate-free model) and final (covariate model) population pharmacokinetic models was performed using bootstrap resampling because of the limited number of patients in the study.

The one-compartment model with an additive error model including IOV in CL was selected as the population model during model development. The final population pharmacokinetic model built in the study was fitted to the 200 bootstrap samples. The mean parameter estimates obtained with the 200 bootstrap replicates of the data were within 15% of those obtained from original data. This indicates that the final model is stable.

With regard to the effect of covariates investigated in this analysis on the pharmacokinetic parameters of busulfan after intravenous infusion, the ABW was found to be a
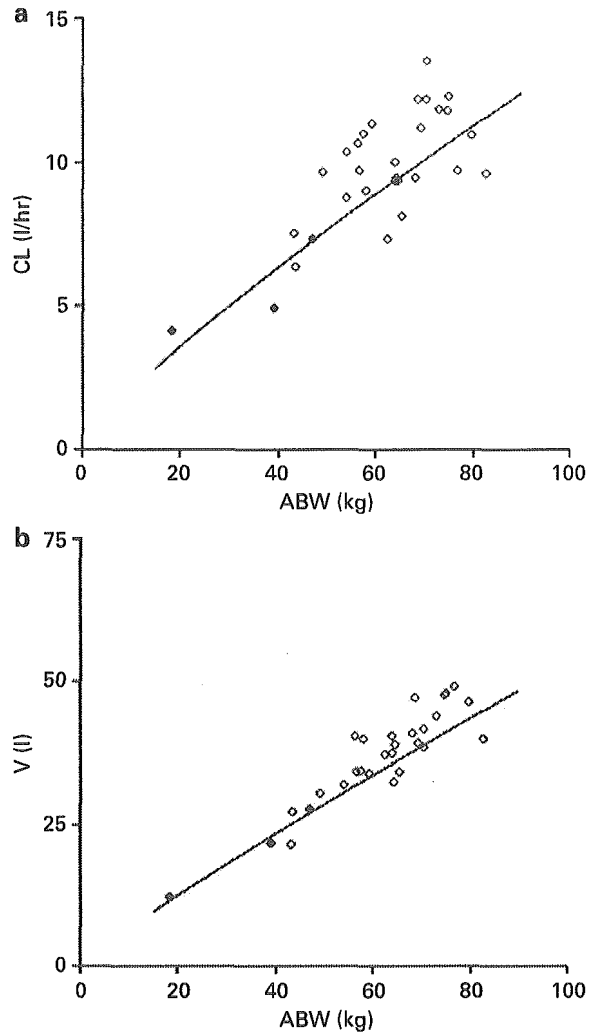
Figure 3 Plots of individual parameter values versus actual body weight. ABW, actual body weight. Clearance (CL) (a) and the volume of distribution (V) (b) after the first administration were calculated according to noncompartmental analysis using WinNonlin. Lines represent the estimates predicted the proposed allometric equations. Open and closed circles represent the value in adults and children, respectively.

determinant of CL and V. In the previous studies, age, ABW, body surface area (BSA), ALT and concomitant phenytoin treatment were reported as possible covariates of oral busulfan pharmacokinetics.[5–9,20,21] After the intravenous administration of busulfan, the relationships between ABW and pharmacokinetic parameters were reported.[13] Since physiological function was relatively well controlled in our study, variation of covariates was in a narrow range or within the normal limits. The limitation of developing population models based on such a small, relatively uniform patient population has been reported.[22] Therefore, the relationships between covariates and the pharmacokinetic parameters of intravenous busulfan need further investigation in a larger population, especially in younger children.

In general, a nomogram based on the population approach is a useful tool for dose adjustment, and therapeutic drug monitoring (TDM) is another powerful